1975-09

Some design experiments for a nested grid forecast model of western Pacific tropical cyclones.

Ley, Gary William

Monterey, California. Naval Postgraduate School

SOME DESIGN EXPERIMENTS FOR A NESTED GRID FORECAST MODEL OF WESTERN PACIFIC TROPICAL CYCLONES

Gary William Ley

NAVAL POSTGRADUATE SCHOOL
Monterey, California

THESIS

SOME DESIGN EXPERIMENTS
FOR A NESTED GRID FORECAST MODEL OF
WESTERN PACIFIC TROPICAL CYCLONES

by

Gary William Ley

September 1975

Thesis Advisor: R. L. Elsberry

Approved for public release; distribution unlimited.

SECURITY CLASSIFICATION OF THIS PAGE (When Data Entered)

REPORT DOCUMENTATION PAGE

READ INSTRUCTIONS BEFORE COMPLETING FORM

1. REPORT NUMBER	2. GOVT ACCESSION NO.
3. RECIPIENT'S CATALOG NUMBER	
4. TITLE (and Subtitle) Some Design Experiments for a Nested Grid Forecast Model of Western Pacific Tropical Cyclones	5. TYPE OF REPORT & PERIOD COVERED Master's Thesis September 1975
6. PERFORMING ORG. REPORT NUMBER	
7. AUTHOR(s) Gary William Ley	8. CONTRACT OR GRANT NUMBER(s)
9. PERFORMING ORGANIZATION NAME AND ADDRESS Naval Postgraduate School Monterey, California 93940	10. PROGRAM ELEMENT, PROJECT, TASK AREA & WORK UNIT NUMBERS
11. CONTROLLING OFFICE NAME AND ADDRESS Naval Postgraduate School Monterey, California 93940	12. REPORT DATE September 1975
	13. NUMBER OF PAGES 72
14. MONITORING AGENCY NAME & ADDRESS(if different from Controlling Office) Naval Postgraduate School Monterey, California 93940	15. SECURITY CLASS. (of this report) Unclassified
	15a. DECLASSIFICATION/DOWNGRADING SCHEDULE

16. DISTRIBUTION STATEMENT (of this Report)

Approved for public release; distribution unlimited.

17. DISTRIBUTION STATEMENT (of the abstract entered in Block 20, if different from Report)

18. SUPPLEMENTARY NOTES

19. KEY WORDS (Continue on reverse side if necessary and identify by block number)

Tropical Cyclone Forecast
Nested Grid Model
Western North Pacific Ocean

20. ABSTRACT (Continue on reverse side if necessary and identify by block number)

A three-dimensional, triply nested tropical cyclone forecast model was initialized from hand-analyzed synoptic-scale wind data. The diagnostic phase forced the mass fields from the wind fields by use of a suitable balance equation. Latent heat parameterization and frictional dissipation were omitted from the model to study movement primarily due to advective processes. For comparison, a three-level uniform coarse mesh grid model was initialized with the same real data. Time averaging of the pressure gradient

DD FORM 1 JAN 73 1473 EDITION OF 1 NOV 65 IS OBSOLETE
S/N 0102-014-6601 |
(Page 1)

SECURITY CLASSIFICATION OF THIS PAGE (When Data Entered)

terms of the momentum equations was incorporated into each model in an attempt to increase the maximum time increment.

Movement forecasts of Typhoon Irma to 48-hours with both dynamic models were compared with operational forecasts and the post-analysis "best" track. Very satisfactory movement prognoses were obtained for the three periods forecasted with the dynamic models. The models correctly forecast the passage of a 500-mb trough to the north of the typhoon, apparently preventing recurvature. For movement forecasts, it appears that the nested model can be initialized with linear interpolation of data from the coarse grid to the finer mesh grids. The time increment was increased through use of the pressure averaging in the uniform CMG model; however, no time step increase was realized with the nested model due to lattice separation of the solution.

SOME DESIGN EXPERIMENTS FOR A NESTED GRID FORECAST MODEL OF WESTERN PACIFIC TROPICAL CYCLONES

by

Gary William Ley
Lieutenant, United States Navy
B.S., The Pennsylvania State University, 1969

Submitted in partial fulfillment of the
requirements for the degree of

MASTER OF SCIENCE IN METEOROLOGY

from the

NAVAL POSTGRADUATE SCHOOL
September 1975

ABSTRACT

A three-dimensional, triply nested tropical cyclone forecast model was initialized from hand-analyzed synoptic-scale wind data. The diagnostic phase forced the mass fields from the wind fields by use of a suitable balance equation. Latent heat parameterization and frictional dissipation were omitted from the model to study movement primarily due to advective processes. For comparison, a three-level uniform coarse mesh grid model was initialized with the same real data. Time averaging of the pressure gradient terms of the momentum equations was incorporated into each model in an attempt to increase the maximum time increment.

Movement forecasts of Typhoon Irma to 48-hours with both dynamic models were compared with operational forecasts and the post-analysis "best" track. Very satisfactory movement prognoses were obtained for the three periods forecasted with the dynamic models. The models correctly forecast the passage of a 500-mb trough to the north of the typhoon, apparently preventing recurvature. For movement forecasts, it appears that the nested model can be initialized with linear interpolation of data from the coarse grid to the finer mesh grids. The time increment was increased through use of the pressure averaging in the uniform CMG model; however, no time step increase was realized with the nested model due to lattice separation of the solution.

TABLE OF CONTENTS

LIST OF FIGURES

LIST OF SYMBOLS

t	Time variable
u	Velocity component in the x-direction
v	Velocity component in the y-direction
x,y	West-east, north-south space axes
θ	Potential temperature
f	Coriolis parameter
τ_{xx}, τ_{yx}	Components of shear stress per unit area by u wind component
τ_{xy}, τ_{yy}	Components of shear stress per unit area by v wind component
M	Map factor
ϕ	Geopotential height
ϕ_{1000}	Geopotential height of 1000 millibar surface
ω	Vertical velocity in pressure coordinates
P	Pressure (space axis in vertical)
θ	Potential temperature
C_p	Specific heat at constant pressure
Δ	Finite difference operator
R	Gas constant for dry air
ρ	Atmospheric density
$\bar{S}$	Average of S over the entire grid
$\tilde{S}$	Average of S along one row of the grid
α	Specific volume
∇^2	Laplacian operator

ACKNOWLEDGEMENT

The author wishes to express his sincere appreciation to Professor R. L. Elsberry for his patient guidance during the course of this research.

The author extends his gratitude to Professor R. T. Williams for his helpful comments and review of the manuscript.

A special appreciation is extended to the W. R. Church Computer Center personnel who provided the numerical support.

A warm thank you is extended to the author's wife, Gigi, for her patience, devotion and unyielding support throughout the period of research.

I. INTRODUCTION

Accurate and timely prediction of tropical cyclone movement and intensity continues to be one of the most difficult realizations in the meteorological community. One reason for the absence of good numerical guidance is that the relatively large grid spacing used in today's numerical forecast models cannot resolve the tropical cyclone circulation. The application of a 381-kilometer (km) grid, such as that used by the Fleet Numerical Weather Central (FNWC), Monterey, California, not only enhances the phase error in short-wave systems, but also lacks the resolution necessary to describe tropical cyclone energetics.

Consequently, successful numerical simulation of mesoscale weather systems will require a finer grid resolution than that currently used in extratropical models. This extra resolution could be achieved by decreasing the grid increment of the mid-latitude model to properly define the mesoscale processes important to tropical cyclone development. However, necessary computer storage and model run time would be prohibitive. For example, for each reduction of the grid spacing by a factor of two, the computer time necessary to generate a forecast at the same temporal point is increased eight-fold. One alternative to a uniform fine mesh model is the use of multiple (nested) grid models. These models incorporate a smaller grid interval only in the immediate vicinity of the disturbance and utilize a coarser mesh grid elsewhere. An example is the three-level primitive-equation, triply nested model of Harrison (1973). Figure 1 shows the grid nesting used in Harrison's model. Typically, the coarse

mesh grid (CMG) resolution is double that of the medium mesh grid (MMG). Likewise, the reduction of the grid spacing from the MMG to the fine mesh grid (FMG) is one-half. Clearly, the advantage of Harrison's (1973) nested model over one that employs a uniform fine mesh grid over its entire domain, is the considerable savings of model run time and computer storage.

Harrison's (1973) experiments were based upon analytically derived initial states. He found that heating in the FMG only, resulted in cyclonic development in the CMG. This development demonstrated that his two-way interaction between grids, will allow for momentum and heat transfer with only minimal effect on the solution. This important achievement sets the stage for more sophisticated and diversified testing of the Harrison model.

It is the purpose of this thesis to continue experiments on Harrison's model, directed toward the eventual development of an operational tropical cyclone forecast model for the western North Pacific. The primary goal of this thesis is to test Harrison's (1973) model using operational real data obtained from the Fleet Weather Central/ Joint Typhoon Warning Center (FWC/JTWC) Guam, Mariana Islands. The storm selected for this study was Typhoon Irma during the period 25 to 27 November 1974. Throughout this time span, Irma's location with respect to synoptic-scale features was such that recurvature was a distinct possibility. Movement forecasts using the nested model and a uniform CMG model (unnested) will be examined to see if numerical guidance would have assisted the forecasters. It was anticipated that one of the primary tests would involve the suitability of the western Pacific data network.

A real data initialization for a nested tropical cyclone model entails numerous general problem areas, the foremost of which is the procurement of data. Mathur (1974) produced a 96-hour movement forecast of Hurricane Isbel (1964) utilizing a nested version of Krishnamurti's (1973) model. His data was hand analyzed on the fine mesh grid scale, with the coarse mesh grid values extracted from the coincident fine mesh grid points. Such an initialization is ideal. That is, a model which forecasts mesoscale weather phenomena may be expected to perform best if real data were readily available on that scale. However, such is not the case in the western Pacific. A successful tropical cyclone model for this region must rely primarily on the synoptic scale for its data base. Then, this data will have to be interpolated to the finer mesh grids. If the storm is readily accessible, aircraft reconnaissance could support the initialization through collection of mesoscale data in the immediate vicinity of the cyclone. Assuming this data can be input to the model in a timely fashion, it would provide an excellent supplement to the synoptic-scale information. However, due to decreasing reconnaissance resources, the likelihood that sufficient mesoscale data can be collected is in question. Thus, initialization of Harrison's model will be attempted using hand analyzed synoptic-scale data extracted onto a 220-km grid. This CMG data will then be linearly interpolated to the finer mesh grids.

A secondary objective of this thesis is to institute study of the feasibility of increasing the time step in Harrison's model. It was stated previously that the nested model's increased resolution near the storm vortex will necessitate increased model run time. This time

increase must somehow be reduced if the model is to be used operationally. Shuman (1971) and Brown and Campana (1971) found that by applying a weighed time average to the pressure gradient term of the momentum equations, the maximum time step could be doubled. Clearly, successful application of this scheme to the nested model would help alleviate the increased time burden. Thus, Harrison's model was re-aligned to accept the time averaging scheme. Since the proposed scheme was not successful for nested versions, only a summary of the results will be presented in the Appendix.

II. PRIMITIVE EQUATION PREDICTION MODEL

A. THE MODEL EQUATIONS

The primitive-equation model after Harrison and Elsberry (1972) and Harrison (1973) was the basis for these experiments. The model equations are:

$$\frac{\partial u}{\partial t} = -L(u) + fv - M\frac{\partial \phi}{\partial x} + \frac{\partial \tau_{xx}}{\partial x} + \frac{\partial \tau_{yx}}{\partial y} , \tag{1}$$

$$\frac{\partial v}{\partial t} = -L(v) - fu - M\frac{\partial \phi}{\partial y} + \frac{\partial \tau_{xy}}{\partial x} + \frac{\partial \tau_{yy}}{\partial y} , \tag{2}$$

$$\frac{\partial \theta}{\partial t} = -L(\theta) , \tag{3}$$

$$\frac{\partial \phi_{1000}}{\partial t} = -L(\phi_{1000}) , \tag{4}$$

$$\frac{\partial \omega}{\partial p} = -M^2\left[\frac{\partial}{\partial x}\left(\frac{u}{M}\right) + \frac{\partial}{\partial y}\left(\frac{v}{M}\right)\right] , \tag{5}$$

$$\frac{\partial \phi}{\partial p} = \theta\, C_p \frac{\partial}{\partial p}\left(\frac{p}{1000}\right)^{R/C_p} , \tag{6}$$

where

$$L(S) = M^2\left[\frac{\partial}{\partial x}\left(\frac{us}{M}\right) + \frac{\partial}{\partial y}\left(\frac{vs}{M}\right)\right] + \frac{\partial}{\partial p}(\omega s)$$

L(S) represents the flux divergence of the general scalar quantity S. Other meteorological symbols used above can be found in the "List of Symbols."

The linear computational stability criterion for two-dimensional equations governing simple wave motion is

$$\frac{C\Delta t}{\Delta x} \leq .707 \tag{7}$$

where

$C \equiv$ the phase velocity of the fastest gravity wave

$\Delta t \equiv$ time increment

$\Delta x \equiv$ horizontal grid increment

Equation (7) dictates a maximum time step of 480 seconds in the nested CMG and the uniform CMG model. The MMG and FMG maximum time steps are 240 and 120 seconds. An increase in the uniform CMG time increment to 800 seconds was achieved by time averaging the pressure gradient term of the momentum equations (see Appendix).

The initial step was forward in time. All subsequent iterations used the leapfrog scheme. Parameterization of heating and moisture was intentionally neglected from the system to emphasize storm movement primarily by advective processes.

B. THE GRID

The grid utilized for this experiment followed that of Harrison (1973). It is a mercator secant projection true at 22.5°N. One can see from Fig. 1 that the grid extends from 100E to 154E and from the Equator to 38N. Figure 1 also illustrates the relative position of the nested model's MMG and FMG at the beginning of the integration on 25 November 1974. The grid mesh for the uniform CMG and the CMG of the nested model was 220 km. Resolution on the nested model's MMG and FMG was 110 km and 55 km, respectively. Figure 2, shows the vertical distribution of dependent parameters for both models. Although the variables are staggered in the vertical, horizontal space staggering was not utilized in these experiments.

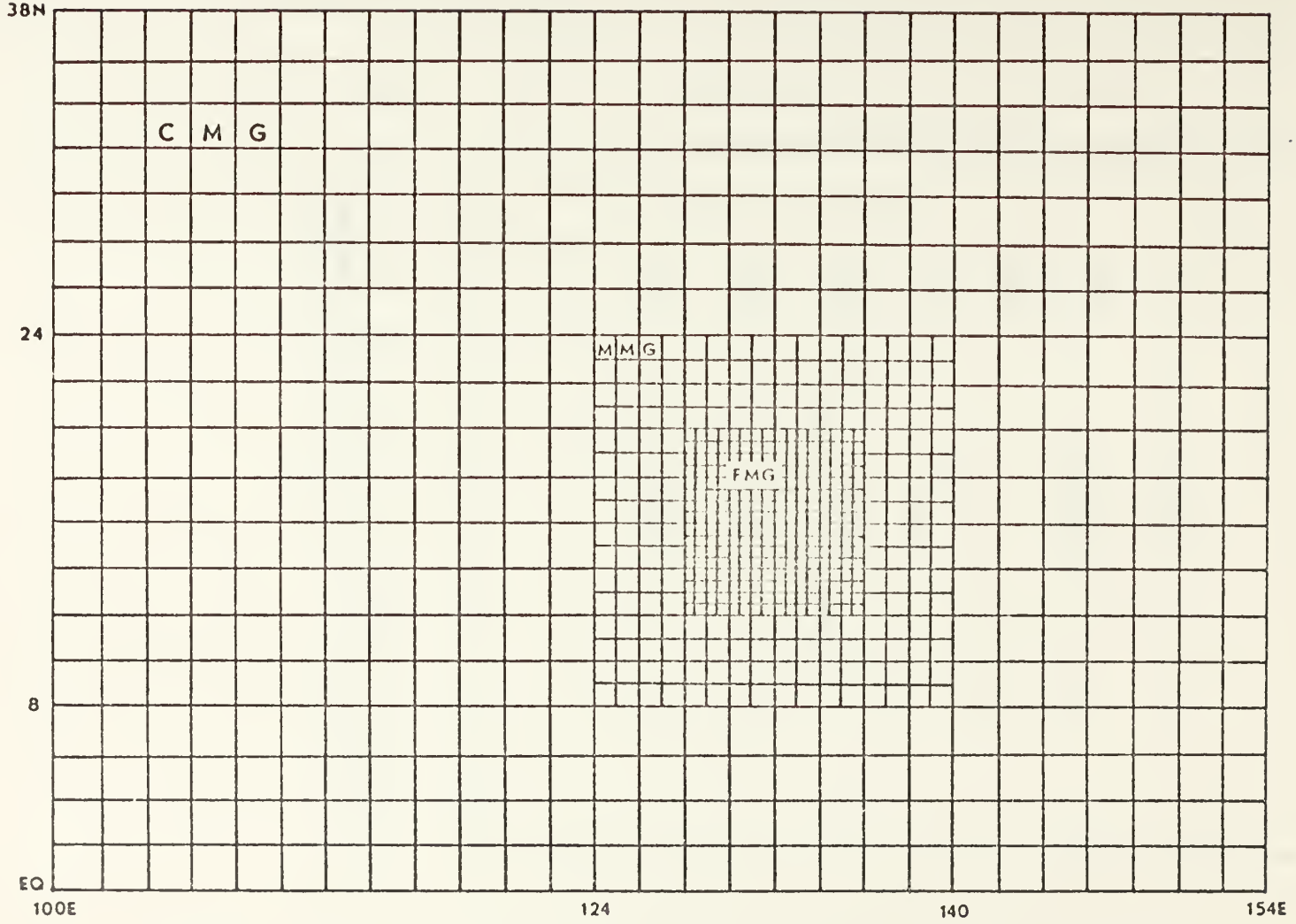

Figure 1. The triply nested grid as it appeared on 00 GMT 25 November 1974. CMG grid spacing is 220 km, MMG spacing is 110 km and FMG increment is 55 km (after Harrison, 1973).

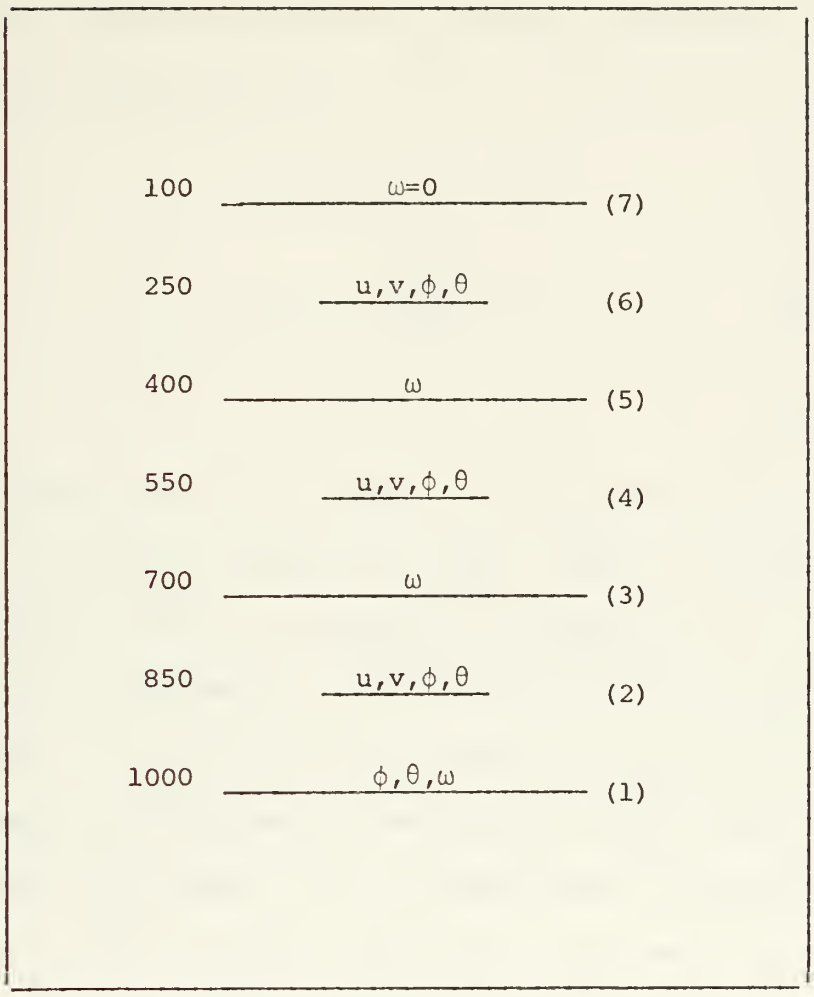

Fig. 2. Vertical distribution of dependent variables and pressure levels for the three-dimensional model (after Harrison, 1973).

C. BOUNDARY CONDITIONS

Boundary conditions on the northern and southern walls for the uniform CMG and nested CMG were the no-flux type after Elsberry and Harrison (1971). These conditions are

$$\phi_{j+1} = \phi_j \tag{8a}$$

$$v_{j+1} = - \frac{M_{j+1}}{M_j} v_j \tag{8b}$$

$$u_{j+1} = u_j \tag{8c}$$

Such representation actually places the wall between the outer two grid rows on the poleward and equatorial sides. Mass is conserved along these boundaries since the v component is always zero at the wall, that is, the wall is a streamline. Thus, the 18 grid rows of extracted data were expanded to 20 rows with the inclusion of the no-flux boundaries.

The east-west boundaries were made cyclic after Krishnamurti (1969). This procedure, applicable to the 1000-mb height field and the 850-, 500-, and 200-mb u,v fields, adds a buffer zone in the east-west direction to absorb the impact of forced continuity. The original data of 23 longitudinal columns was expanded to 28 columns by adding one column to the west side and four columns to the east side. The filling of this buffer is accomplished letting

$$S_{28,j} = S_{2,j} \tag{9a}$$

$$S_{1,j} = S_{27,j} \tag{9b}$$

and then linearly interpolating to fill values in columns 25, 26 and 27. Here S represents any of the original data fields mentioned earlier.

The vertical velocity at the upper boundary is equal to zero and is calculated at levels 5, 3 and 1, Fig. 2, through downward integration of Eq. (5). Optimum results were obtained when, in Eq. (4), $\omega \frac{\partial \phi}{\partial p}$ was replaced by the equivalent expression $-\omega\alpha$. Further solution improvement was attained when ω in Eq. (4) was represented by an averaged value from

$$\omega_{ij} = (\omega_{i,j+1} + \omega_{i,j-1} + \omega_{i+1,j} + \omega_{i-1,j} + 4\omega_{i,j})/8 \qquad (10)$$

D. DIFFUSION

Horizontal diffusion is a computational device that was used to control small scale instability, to retard lattice solution separation and to remove high frequency noise from the model solution. It was not intended to represent parameterization of a physical atmospheric process, but rather to be utilized as a higher order smoothing mechanism. The diffusion components in the u momentum equation are

$$\frac{\partial \tau_{xx}}{\partial x} = \rho K_H \frac{\partial^2 u}{\partial x^2} \qquad (11a)$$

$$\frac{\partial \tau_{yx}}{\partial y} = \rho K_H \frac{\partial^2 u}{\partial y^2} \qquad (11b)$$

Here K_H is the horizontal diffusion coefficient. A similar representation of diffusion was applied to Eq. (2)。 In the uniform CMG model, $K_H = 1 \times 10^5 m^2/sec$, provided the best results. This coefficient was carefully chosen, because a value too large will smooth the meteorological modes as well as the spurious $2\Delta x$ and $3\Delta x$ waves. In the nested model, $K_H = 4 \times 10^5 m^2/sec$, was used on the MMG. The FMG value was

$K_H = 1 \times 10^5 m^2/sec$. The difference by a multiple of four arises due to the dependence of the diffusion on the grid increment (see Eq. (11a)). No horizontal diffusion was used in the nested model CMG. Likewise, no vertical diffusion or frictional effects at the surface have been incorporated into either model.

E. FILTER

Prior to output, the 1000-mb geopotential and wind velocity fields at all levels were smoothed twice with Shapiro's (1971) "ideal" 9-point filter. The advantage of this particular filter is that it completely removes $2\Delta x$ waves and most of the $3\Delta x$ modes. The filter is described generally by:

$$\bar{\alpha} = \frac{1}{16}[2(\alpha_{i+1,j} + \alpha_{i-1,j} + \alpha_{i,j+1} + \alpha_{i,j-1}) + 4\alpha_{i,j} + \alpha_{i+1,j+1} + \alpha_{i-1,j+1} + \alpha_{i+1,j-1} + \alpha_{i-1,j-1}] \quad (12)$$

It was not employed during the integration process to avoid smoothing the meteorological waves.

III. NESTED GRID INTERACTION AND GRID MOVEMENT

A. TWO-WAY INTERACTION VS ONE-WAY INTERACTION

The primary feature that distinguishes nested grid models is the nature of the interaction between grid scales. Information can be passed between the different grid scales by either one-way interaction or two-way interaction (Phillips and Shukla, 1973). With one-way interaction, the larger scale solution determines the smaller scale motion, without being influenced by the changes occurring within the finer mesh grid. The iterative procedure is simple, since the grids are integrated separately using the same coding. This type of boundary best fits situations where the large scale physics are passive with respect to those on the smaller scale. That is, one-way interaction simply provides increased resolution with no feedback from the FMG to the CMG.

It is well documented from previous studies, that an integral part of the tropical cyclone development process is the energy transfer from the small scale convective towers to the synoptic scale (convective instability of the second kind (CISK)). If a numerical model is to simulate the tropical cyclone energetics, it too should provide a means for energy transfer among the various scales of motion. Obviously, since the smallest mesh length in the Harrison model is 30 nmi, energy transfer from the cloud scale to the mesoscale cannot be parameterized; however, the two-way interaction inherent in the model does allow for transfer of energy between the mesoscale (FMG) and synoptic scale (CMG).

Two-way interaction, such as that used by Harrison (1973), requires simultaneous integration on all grids. Figure 3 illustrates this integration procedure. One can see that first the CMG is integrated one time step, then the MMG, then the FMG two steps, the MMG again and finally two more FMG iterations. This formal procedure is necessary since each reduction in the grid increment requires a corresponding change in the time step (Eq. (7)) and all grids must be at the same temporal location prior to the next CMG iteration. After each integration of the coarser mesh grid, the boundaries on the finer mesh grid are specified through temporal and spatial interpolation of the corresponding coarse grid values. At the conclusion of every FMG integration, the interior coincident grid points in the MMG grid are revised via a nine-point average. The same procedure is used to update the CMG with the MMG solution. Thus, the coarser grid provides the boundary values to the finer grid, which, upon completion of the finer mesh grid integration, feeds back new values to the interior of the coarse grid.

B. MOVEMENT OF THE NESTED GRIDS

Successful movement of the finer mesh grids within their coarser counterparts is a necessary condition that must be fulfilled before long-term tropical cyclone forecasts can be generated with a nested model. The best solution on the FMG should be obtained if the storm being monitored remains near the center of the grid. It can be surmised that close proximity of the storm to the grid boundary will lead to a deteriorating solution and possibly even computational instability. The longitudinal distance across the 17 x 17 point FMG with grid resolution of 30 nmi is 510 nmi. A storm initially at the center of the grid

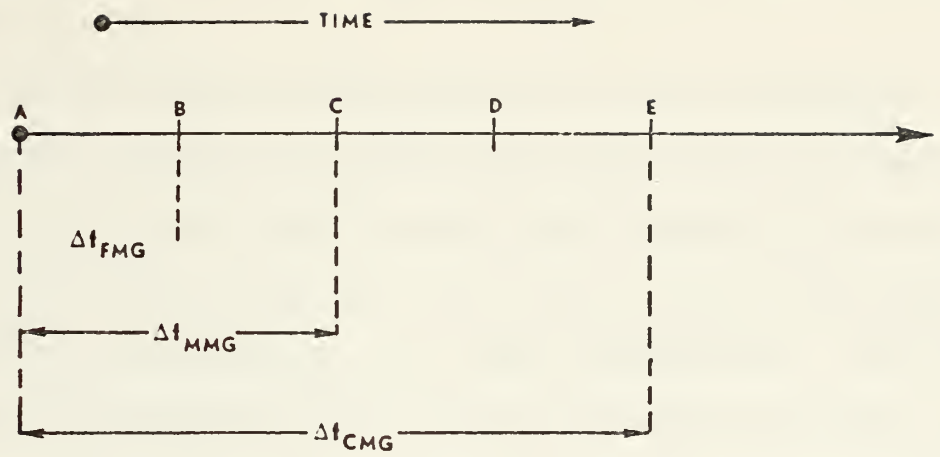

Figure 3. A schematic to illustrate the marching process in a nested grid model (Harrison, 1973).

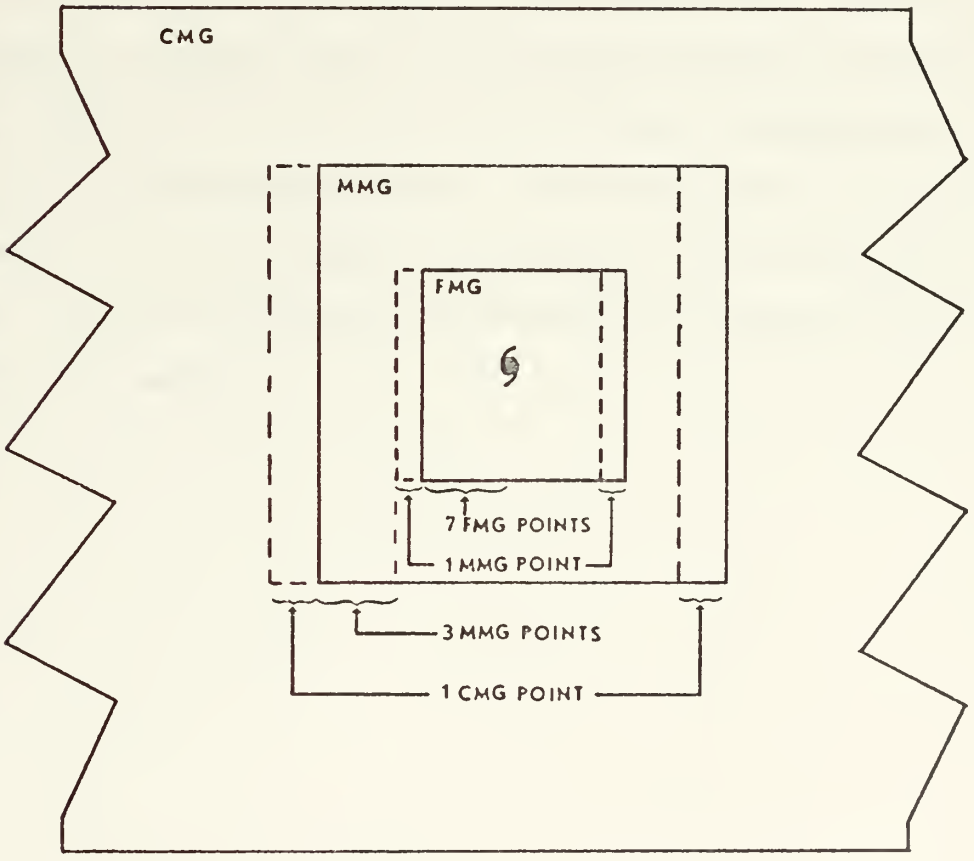

Figure 4. An illustration of MMG and FMG movement.

will reach the west edge in one day, assuming a 10-knot average westward speed. Therefore, grid movement is an essential component of the Harrison model.

When the minimum 1000-mb geopotential value corresponding to the approximate storm vortex moves to the seventh grid point from the western boundary of the FMG, the FMG grid is moved one MMG grid point to the west. From Fig. 4, one can see that the procedure entails the placement of the coincident MMG values onto their proper FMG positions. Then linear spatial interpolation is used to fill the remaining FMG voids. The two FMG eastern-most columns are disregarded and the storm center becomes relocated at the ninth FMG point from the west boundary.

If, in turn, the FMG moves to within three grid points of the MMG west boundary, the MMG is moved one CMG point to the west. The new western MMG values are taken from the CMG and linearly interpolated in space to fill the remaining MMG vacancies. Referring to Fig. 4, movement of the MMG in the CMG also requires a redefining of the FMG location within the MMG. Identical provisions are provided for relocation of the FMG and MMG to the north.

IV. INITIALIZATION

A. DATA INPUT

Data for the initialization were supplied by the U. S. Fleet Weather Central/Joint Typhoon Warning Center, Guam, Mariana Islands (FWC/JTWC). The surface pressure and 850-, 500- and 200-mb isotachs and streamlines were hand-analyzed at 00 GMT 25, 26 and 27 November 1974. These analyses, plus the careful extraction of the data to the grid, provided a data base superior to objective analyses which might have been available.

For convenience, the real atmospheric data at 500- and 200-mb were extracted to the nearest model predictive level (see Fig. 2). Subsequent reference to these levels will be according to the real data level, not the model's predictive level.

B. TROPICAL VS EXTRATROPICAL

In general, initialization of tropical models differs from their extratropical counterparts. In a mid-latitude model, the wind is normally derived from a solution of the balance equation with an objectively analyzed geopotential field (Haltiner, 1971). Such a procedure is not suitable for a tropical model since the pressure gradient in the southern latitudes is very weak and the pressure field is not well defined. Moreover, it can be shown that the mass field primarily tends to adjust to the wind field in the tropics during the early stages of the integration after initialization, especially in mesoscale models as found by Anthes (1974). Consequently, in the tropics, primary consideration must be given to the wind field when performing the initial diagnostic phase.

C. UNIFORM CMG DIAGNOSTIC PHASE

The relative vorticity fields were obtained from the observed u and v components with

$$\zeta_r = M^2 [\frac{\partial}{\partial x} (\frac{v}{M}) - \frac{\partial}{\partial y} (\frac{u}{M})] \tag{13}$$

Subsequently, the streamfunction, ψ, was found by sequential over-relaxation of the expression

$$\nabla^2 \psi = \zeta_r \tag{14}$$

and the non-divergent wind components were calculated through

$$u_\psi = - M \frac{\partial \psi}{\partial y} , \quad v_\psi = M \frac{\partial \psi}{\partial x} \tag{15}$$

Solution of Eq. (14) requires specification of boundary values on the northern and southern peripheries. To remain consistent with the no-flux boundaries, described by Eqs. (8b) and (8c), constant streamfunction values were defined for the northernmost and southernmost two rows. Following Elsberry and Harrison (1971), zero was chosen for the southern rows, and the northern values were calculated from

$$\tilde{\psi}_{north} = \tilde{\psi}_{south} - (\frac{\bar{u}_\psi}{M}) \Delta y \tag{16}$$

Here $\bar{u}_\psi$ is the mean zonal wind component averaged over the entire grid and Δy is the distance between the north and south walls.

An appropriate balance equation can be derived through partial differentiation of Eq. (1) with respect to x and Eq. (2) with respect to y. Addition of these two equations, plus rearrangement of terms leads to

$$\frac{\partial}{\partial t}\left(M^2\left[\frac{\partial}{\partial x}\left(\frac{u_\psi}{M}\right)+\frac{\partial}{\partial y}\left(\frac{v_\psi}{M}\right)\right]\right) = -M^2\left[\frac{\partial}{\partial x}\frac{L(u_\psi)}{M}\right]-M^2\left[\frac{\partial}{\partial y}\frac{L(v_\psi)}{M}\right]+fM^2\left[\frac{\partial}{\partial x}\left(\frac{v_\psi}{M}\right)-\frac{\partial}{\partial y}\left(\frac{u_\psi}{M}\right)\right]$$

$$-M^2 u_\psi \frac{\partial}{\partial y}\left(\frac{f}{M}\right)-M^2\left[\frac{\partial^2\phi}{\partial x^2}+\frac{\partial^2\phi}{\partial y^2}\right] \qquad (17)$$

To begin the prognostic stage smoothly, the left hand side of Eq. (17) is set equal to zero. Surface diffusive effects were neglected. Manipulation of Eq. (17) leads to a Poisson equation,

$$\nabla^2\phi = -\frac{\partial}{\partial x}\left[\frac{L(u_\psi)}{M}\right]-\frac{\partial}{\partial y}\left[\frac{L(v_\psi)}{M}\right]+f\left[\frac{\partial}{\partial x}\left(\frac{v_\psi}{M}\right)-\frac{\partial}{\partial y}\left(\frac{u_\psi}{M}\right)\right]-u_\psi\frac{\partial}{\partial y}\left(\frac{f}{M}\right) \qquad (18)$$

that is readily solved with sequential over-relaxation or other direct methods. In this case, the mean geopotential value on the south wall was derived hydrostatically (Eq. (6)) based upon a mean climatological temperature sounding. An average geopotential value for the north wall was found through integration of the v momentum equation (noting that $\frac{\partial v}{\partial t} = 0$) over the region.

$$\tilde{\phi}_N = \tilde{\phi}_S - \left[\bar{f}\cdot\left(\frac{\bar{u}_\psi}{M}\right)+\frac{\overline{L(v_\psi)}}{M}\right]\Delta y \qquad (19)$$

Again, Δy is the north-south grid distance. To assure maintenance of the no-flux boundary conditions, Eq. (8a) was now applied at all levels. Having found the balanced geopotential fields from the upper level wind fields, only the 1000-mb geopotential field and the temperature fields

at levels 1, 2, 4 and 6, Fig. 2, need to be specified to begin the prognostic phase. Since the initial wind fields are non-divergent, the vertical velocity is everywhere zero.

The 1000-mb geopotential field was obtained hydrostatically from the 850-mb values. This requires that the 1000-mb and 850-mb potential temperature fields are defined. From Eq. (6), recall that the thickness between two levels in the atmosphere is proportional to the mean potential temperature of the layer. Constant potential temperatures for the 1000-mb north and south walls were obtained from climatology. A linear gradient at 1000 mb was forced to fit the boundary values. It was assumed that the 850-mb potential temperatures were everywhere 4°K warmer than the corresponding 1000-mb values. This assumption resulted in a linear meridional gradient in the 1000/850-mb layer mean potential temperature field. Finally, the 1000-mb geopotential field and the 500-mb and 200-mb potential temperature distributions were obtained using Eq. (6).

D. NESTED GRID MODEL DIAGNOSTICS

The diagnostic procedure for the nested model CMG followed that of the uniform CMG model (see Fig. 5). A discussion of the diagnostic phase of the interior grids is now presented. Particular emphasis will be placed on the MMG and FMG initialization.

1. Telescoping

The divergent wind components on the MMG were interpolated linearly from the CMG values. The same interpolation scheme was applied to define the FMG wind distribution. Vorticity fields were calculated on both finer mesh grids. The streamfunction field was saved from the

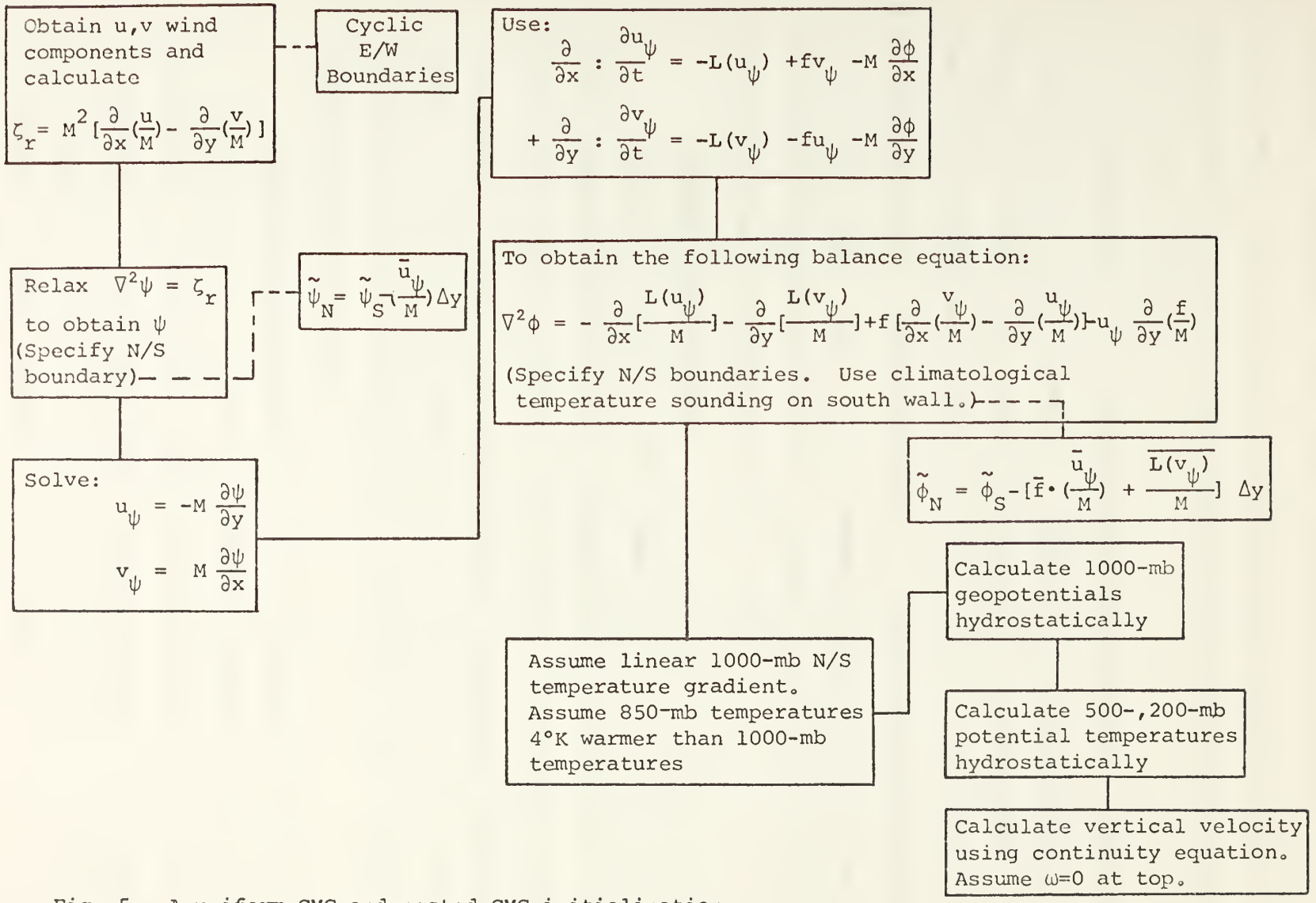

Fig. 5. A uniform CMG and nested CMG initialization.

previously relaxed CMG, and through linear interpolation, provided boundary values and an initial guess field for the solution of Eq. (14) on the MMG. Having calculated the non-divergent wind on the MMG, the FMG streamfunction initial guess field was formed, the solution obtained and the winds computed.

Subsequently, the non-linear balanced equation was solved for the geopotential fields. Again the coarser grid solution provided the boundary values and initial guess fields for the finer mesh grid. The MMG and FMG 1000-mb and 850-mb potential temperature domains were interpolated successively from the coarser grid. The 1000-mb geopotential field and the upper level potential temperature fields for the nested grids were derived hydrostatically. Finally, like the CMG, the MMG and FMG vertical velocity fields were equal to zero.

2. "Reverse" Telescoping

Elsberry and Harrison (1971) found that, in a limited region model, improper specification of the geopotential boundaries may lead to oscillations in the mass field. This "sloshing" results from a mismatch of the boundaries and the wind distribution. To eliminate the possible imbalance caused by the specification of the CMG mass and wind fields as boundary values for the MMG and FMG, a procedure called "reverse" telescoping was introduced.

Reverse telescoping makes use of an enlarged MMG and FMG during the diagnostic phase. Remember that optimum prognostic results would be expected if the model were initialized only from mesoscale data. The application of an expanded grid allows for greater usage of mesoscale data, which hopefully, will lead to minimization of the adjustment during the initial stages of the integration.

The foundation for the reverse telescoping is that during relaxation of a Poisson equation, the effect imposed by the specified boundary values quickly diminishes toward the grid interior. This means that, although the total north-south geopotential gradient may not support the mean wind field between (see Eq. (19)), the interior grid will be consistent with the mean wind field implied by the forcing function. Thus if the MMG and FMG are expanded to a larger size, as in Fig. 6, the initialization within the interior normal 17 x 17 grid boundaries should represent an improved balanced state. MMG and FMG grid expansions to 21 x 21 points were used during the initialization. A still larger grid expansion may be expected to yield higher quality results; however, its use will probably be limited by the large increase in computer storage requirements.

The application of reverse telescoping does not necessitate revision of the telescoping initialization described earlier, except to apply this procedure to the enlarged MMG and FMG. What is required, however, is an extension of the initialization in the reverse direction. After determining the FMG streamfunctions, or geopotential fields, new solutions for the MMG and CMG streamfunction and geopotential fields are calculated with the finer mesh grid values as interior boundaries. Re-application of the relaxation technique is necessary to ensure that the boundary conditions of the finer mesh grid correspond to the values in the coarser mesh grid coincident with the finer grid boundary. This preserves the two-way interaction between grids.

To avoid repetition, the reverse phase will now be described as schematically illustrated in Fig. 7, assuming that the FMG streamfunction

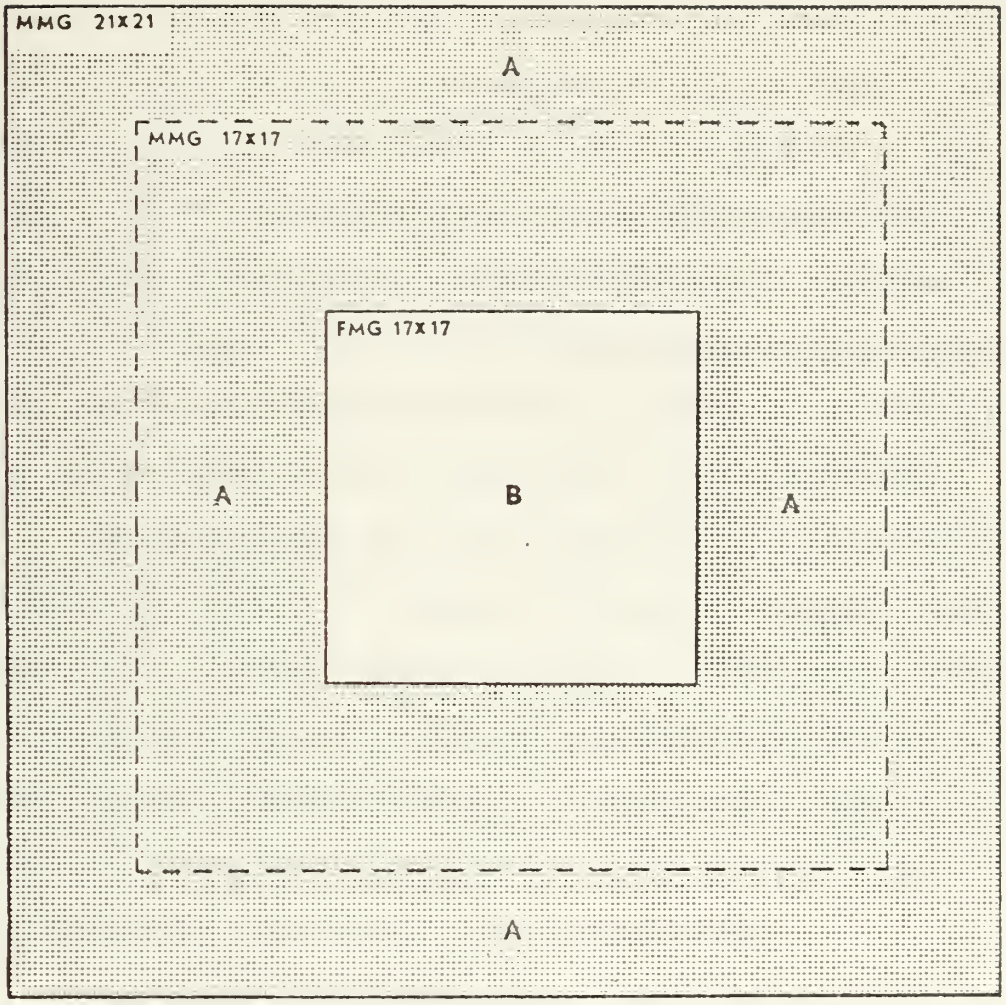

Figure 6. Grid enlargement including depiction of the area relaxed during reverse telescoping.

field has been solved. Subsequently, the inner 17 x 17 FMG streamfunction values and non-divergent winds were extracted and placed at appropriate positions on the MMG. The expanded MMG streamfunction grid was calculated within area A, Fig. 6. This ties the interior streamfunction boundary of the FMG with the remainder of the MMG field, and necessitates recalculation of the MMG non-divergent wind field in area A. Finally, the MMG streamfunction and non-divergent winds were extracted to their proper CMG positions. The CMG streamfunction field was determined within the perimeter area and the corresponding wind field was recomputed. Note, that the procedure required that the vorticity fields on all grids were retained from the telescoping phase of the calculations.

Having finished the reverse procedure for the streamfunction, the method was similarly extended to the balance equation. Here the impact of the "reverse" telescoping should be more profound, because the interpolation of the data to the finer mesh grid was linear, and the balance equation contains several non-linear terms. Note also, that the telescoping phase for the geopotential fields relies on the winds obtained from the reverse telescoping of the streamfunction.

Upon completion of the reverse telescoping only the 17 x 17 MMG and FMG geopotential and wind fields were retained for the prognostic stage. The combination of the telescoping and reverse telescoping phases, plus the remaining diagnostic steps, is summarized in Fig. 7.

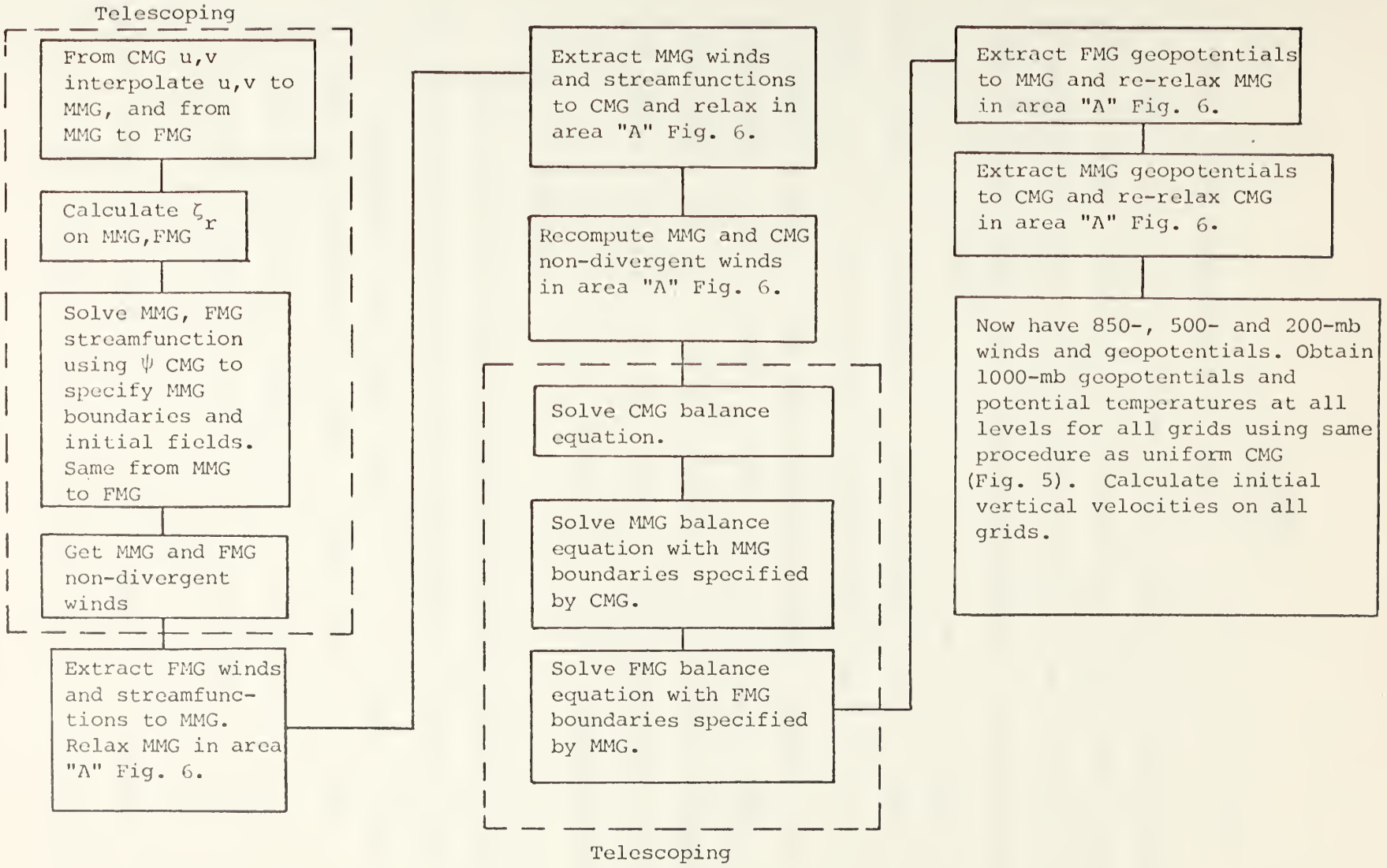

Fig. 7. The telescoping-reverse telescoping procedure.

V. RESULTS

A. INITIAL AND 24-HR PROGNOSTIC FIELDS

Example of the initial streamfunction fields of the triply nested model at 00 GMT 25 November 1974 are presented in Figs. 8-10. Because the reverse telescoping procedure adds increased resolution primarily near the cyclone vortex, the uniform CMG model initial streamfunction distributions are nearly identical to those of the nested model. The massive low-level circulation is well depicted in Fig. 8. Since the models are initialized from hand-analyzed wind fields, there is good vertical consistency in the streamfunction analyses, especially near Typhoon Irma. Other important synoptic features include a moderately strong 500-mb short-wave trough northwest of Irma, and the subtropical high cells east and west of Irma, (Fig. 9). The 200-mb chart, Fig. 10, indicates a weak southeasterly flow over Irma, with no cyclonic vortex present at this stage.

Having noted the similarity between the uniform CMG model non-divergent wind fields with those of the nested model, the effects of the reverse telescoping can be easily identified with the aid of Figs. 11 and 12. One can see the effect of the increased resolution attained near the vortex in the reverse telescoped model (Fig. 12), and the similarity of the fields in regions distant from the storm center. In this case the diagnosis of the mass field from the finer scale wind fields introduces a closed 30-m contour that does not appear on the coarse grid field. The reversed telescoped MMG initial 1000-mb height distribution that

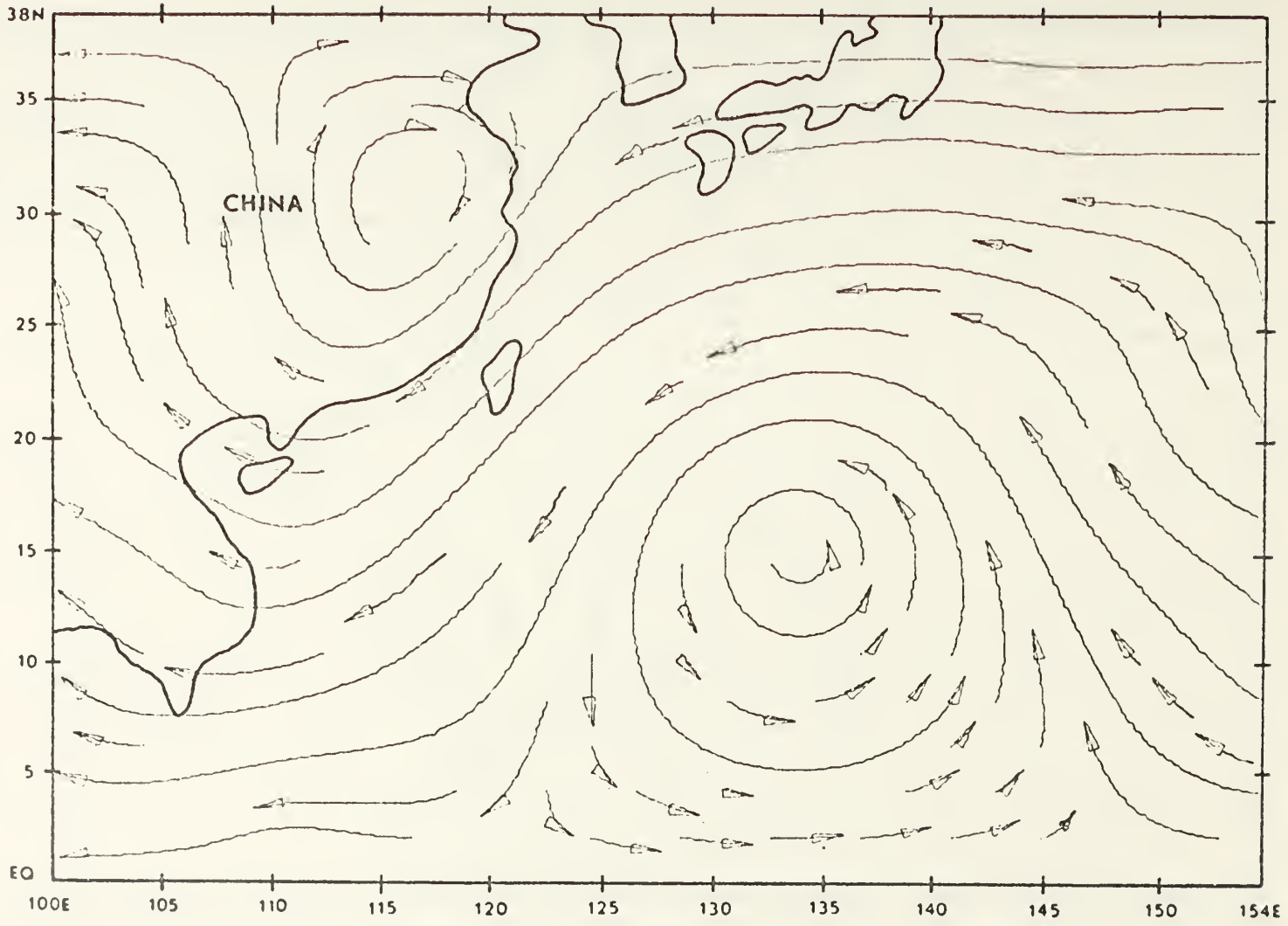

Figure 8. Nested model initial 850-mb streamfunction at 00 GMT 25 November 1974 (reverse telescoping).

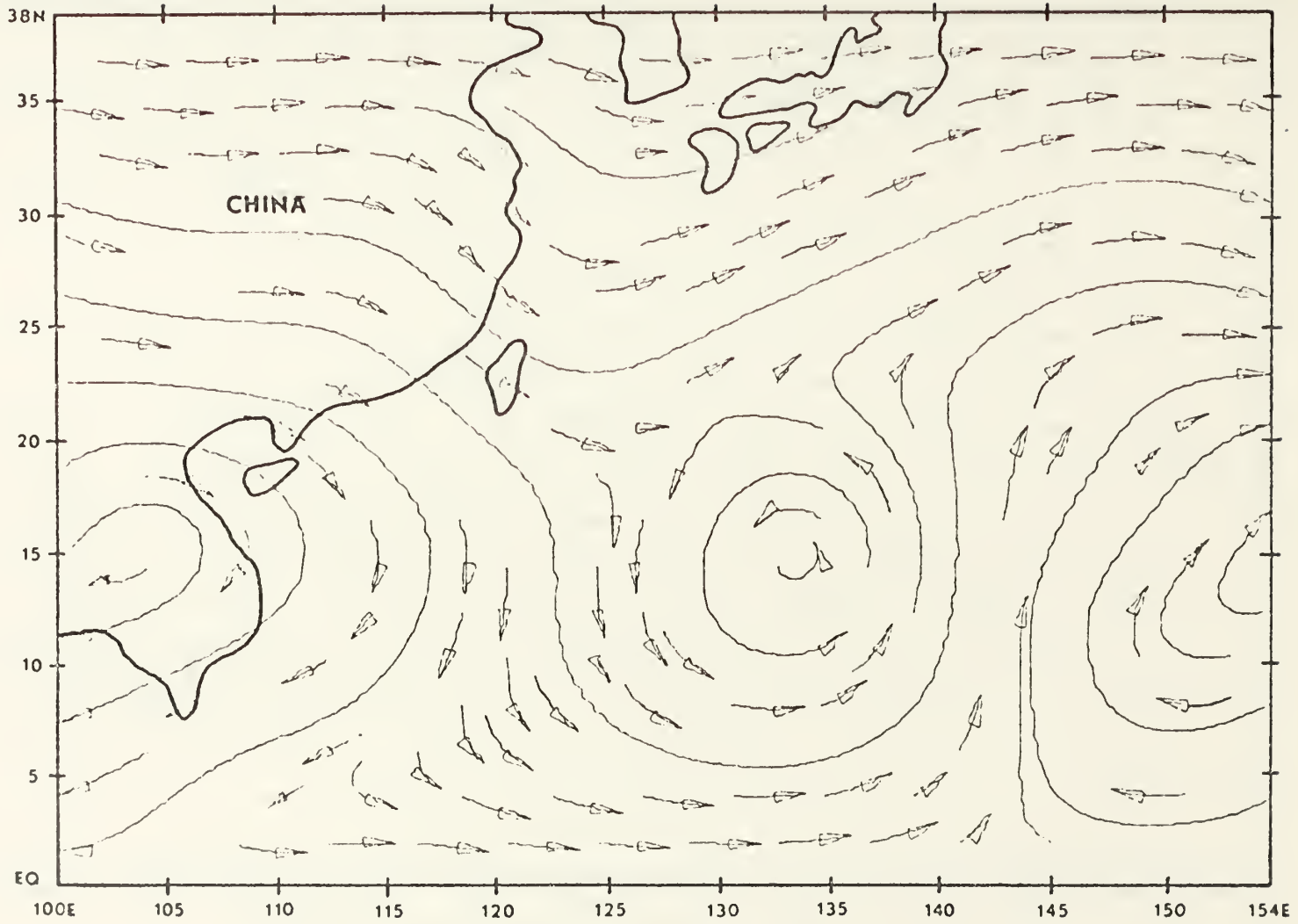

Figure 9. Nested model 500-mb streamfunction at 00 GMT 25 November 1974 (reverse telescoping).

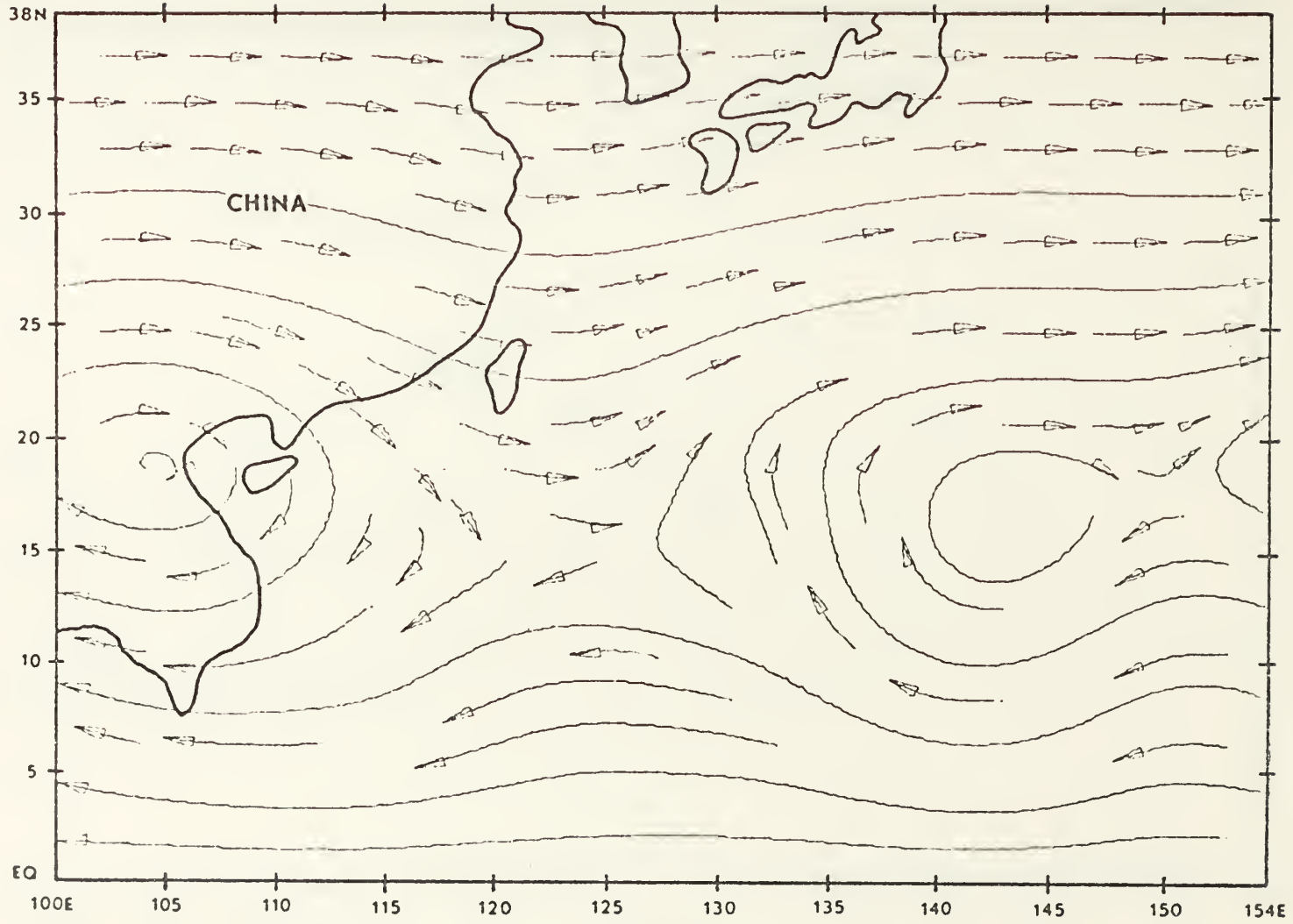

Figure 10. Nested model 200-mb streamfunction at 00 GMT 25 November 1974 (reverse telescoping).

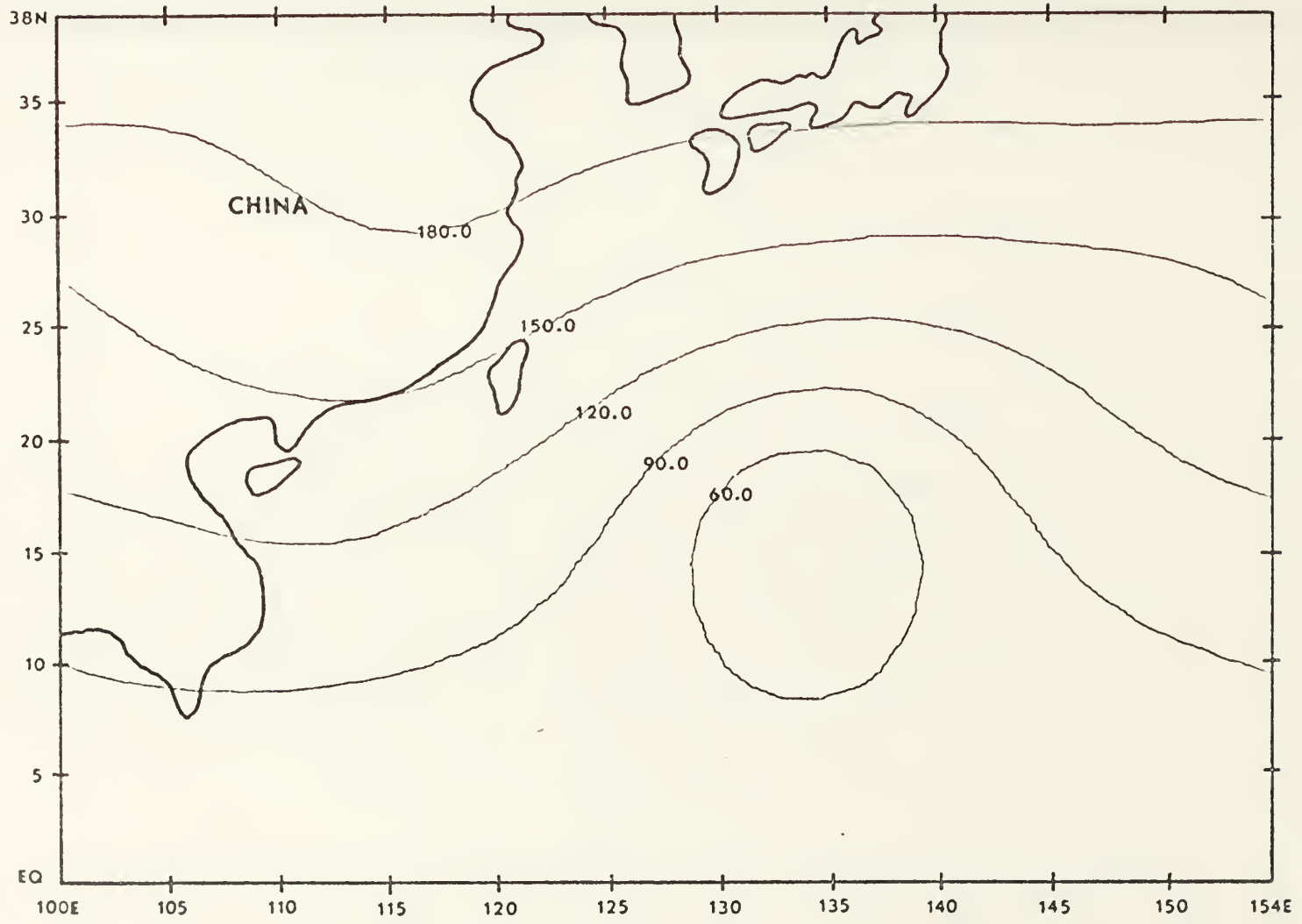

Figure 11. Uniform CMG model 1000-mb height field at 00 GMT 25 November 1974.

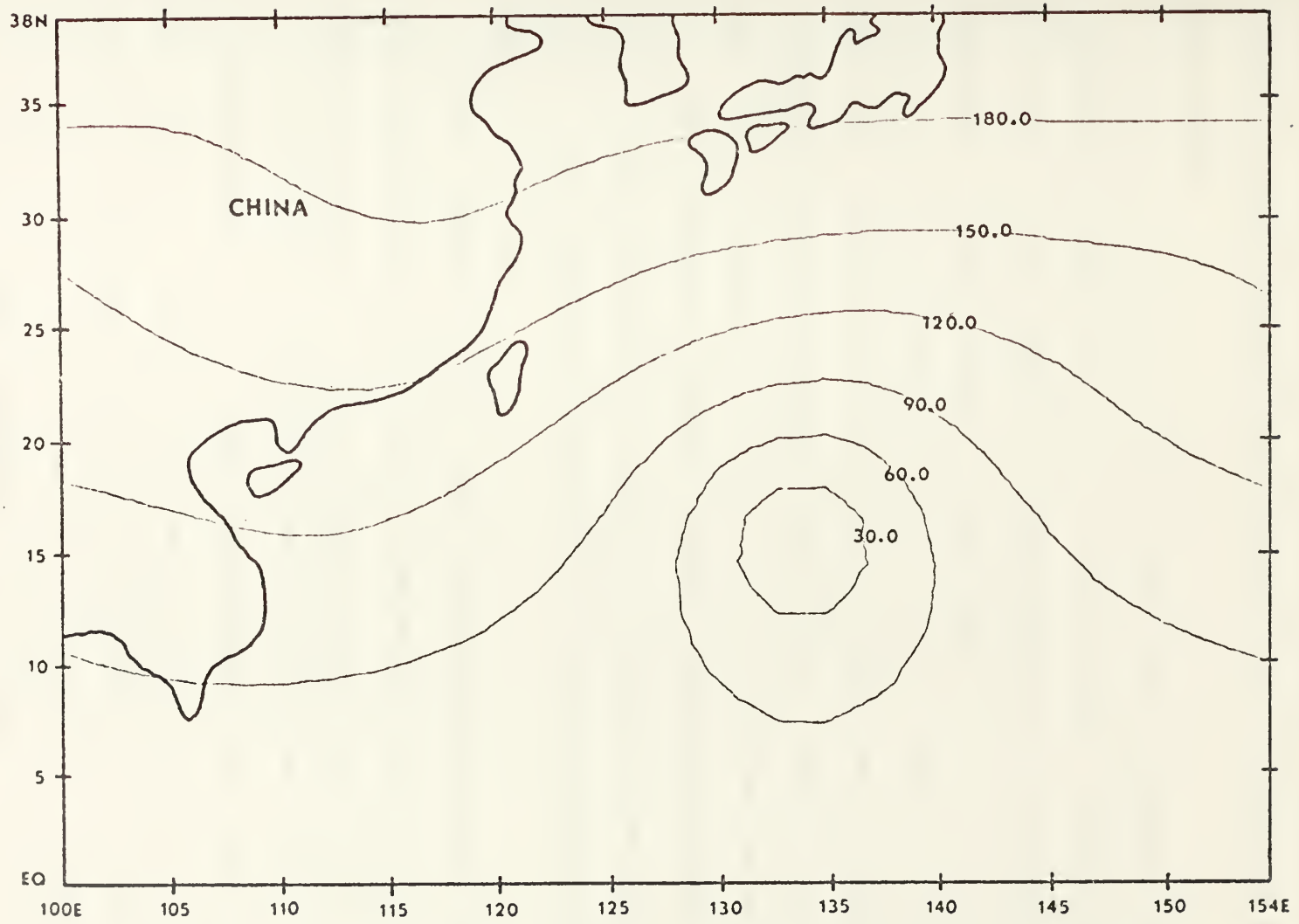

Figure 12. Nested model 1000-mb height field at 00 GMT 25 November 1974 (reverse telescoping).

corresponds to the CMG initial field in Fig. 12, is presented in Fig. 13. Increased definition of the cyclone vortex is clearly depicted here. Note that this grid contains the 0-m and 30-m contours, supporting the fact that the higher resolution of the MMG allows for analysis of finer scale features.

Prognostic fields from the triply nested model verifying at 00 GMT 26 November are shown in Figs. 14-17. In many regards, the large scale wind fields are nearly identical to those prepared with the uniform coarse mesh model. The most significant 24-hour change, is the northeastward building of the 500-mb ridge to the west of Irma, as shown in Fig. 16. This occurs in response to the northerly flow behind the vacating mid-latitude trough observed northwest of Irma earlier. Based on the initial fields, it was expected by operational meteorologists that the advance of the 500-mb trough would produce a northward deflection and cause Irma to recurve into the westerlies. However, recurvature did not occur in the model (or in nature, see next Section) as the mid-latitude trough passed north of Irma.

Careful observation of Figs. 15-17 will reveal some vertical separation in the storm structure. That is, the 24-hour 500-mb forecast position is slightly north of the forecast center at lower levels. This vertical decoupling is caused by the shearing of the mean flow with height, the coarse resolution of the model, and the lack of deep convective heating in the model. Greatest vertical decoupling was observed on 25 November when the equatorward penetration of the westerlies was the greatest. Very little vertical separation was noted for the 24-hour forecast fields from 26 November, possibly suggesting that consistent steering flows

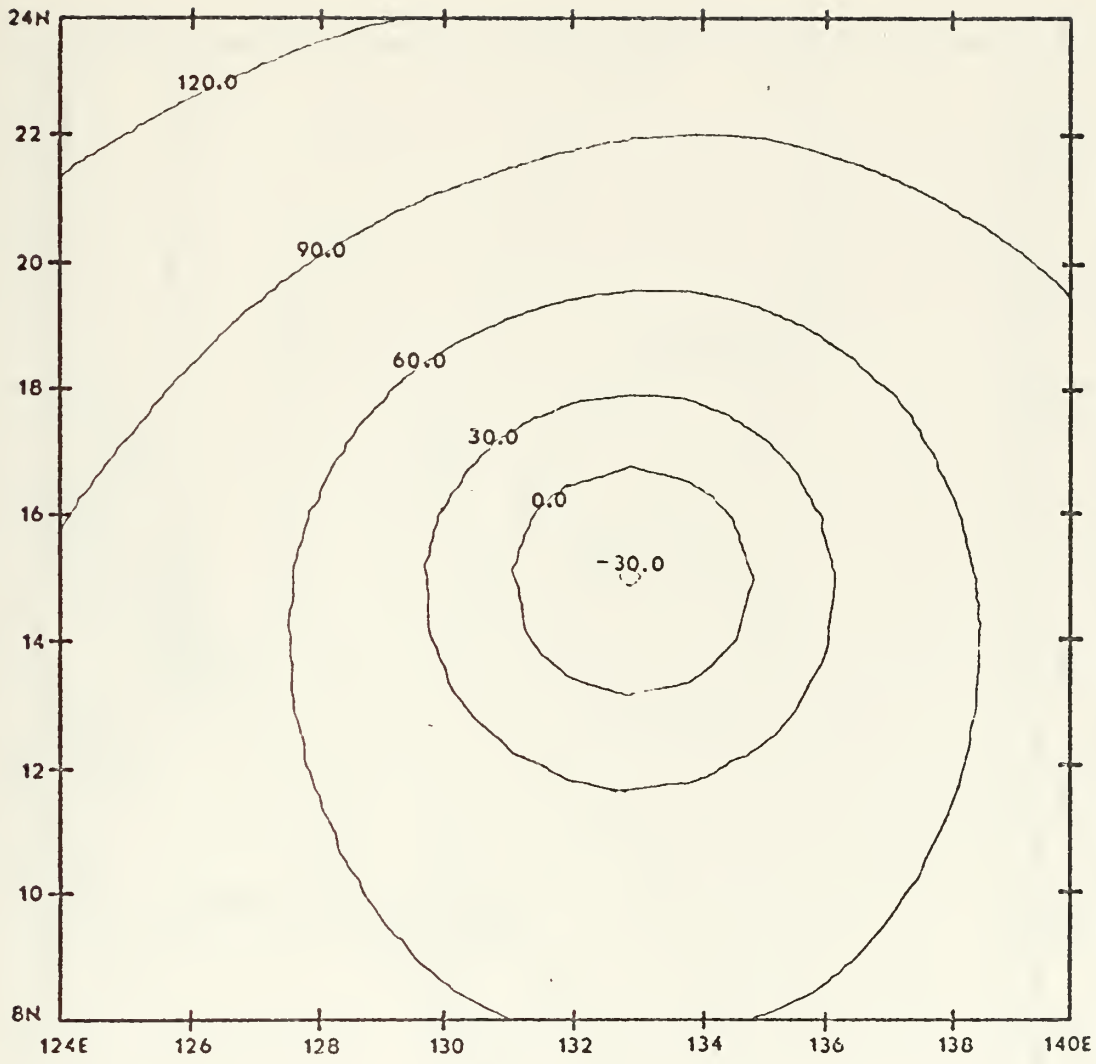

Figure 13. Nested model MMG initial 1000-mb height field at 00 GMT 25 November 1974 (reverse telescoping).

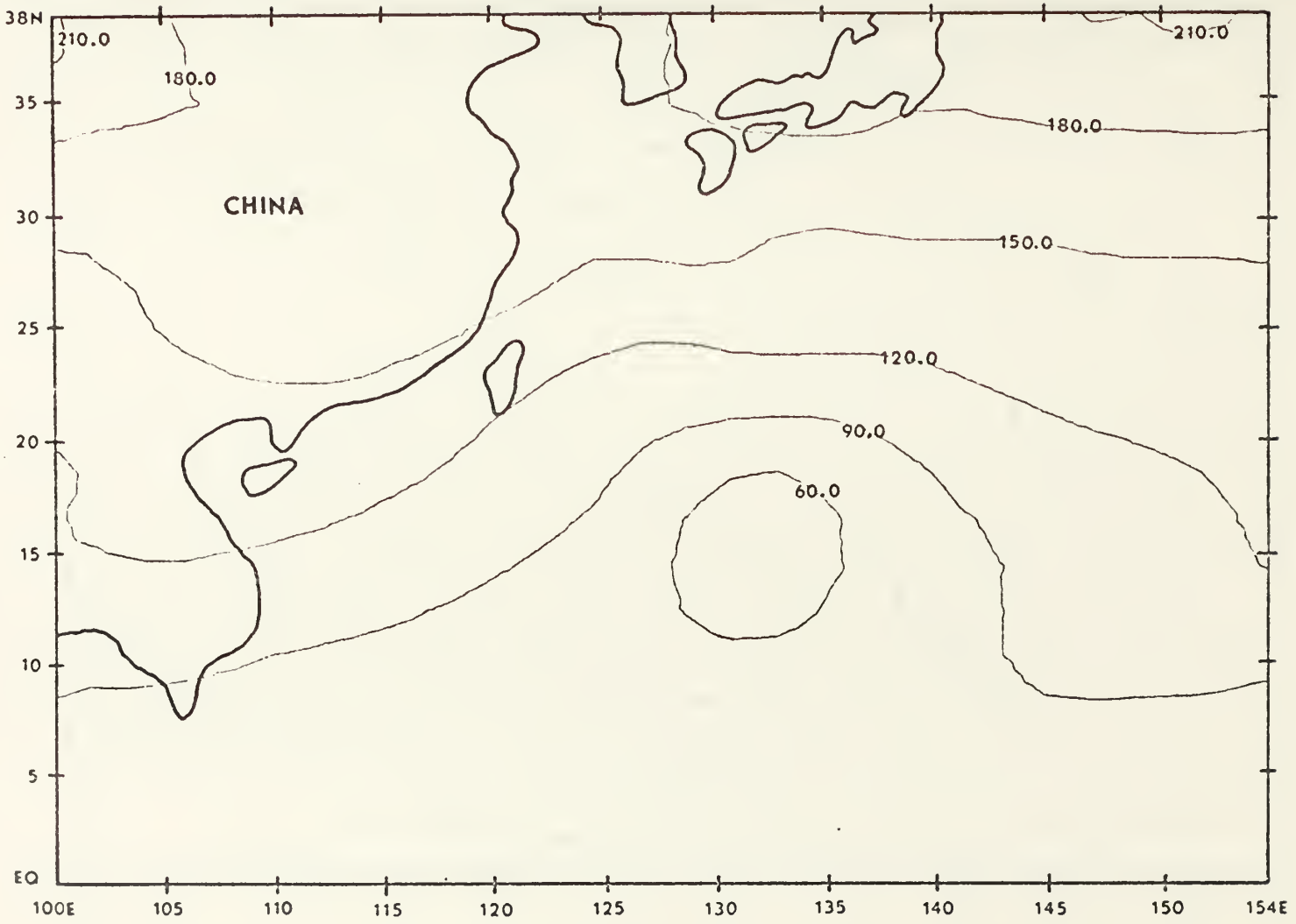

Figure 14. Nested model 24-hour 1000-mb height prognosis from 00 GMT 25 November 1974.

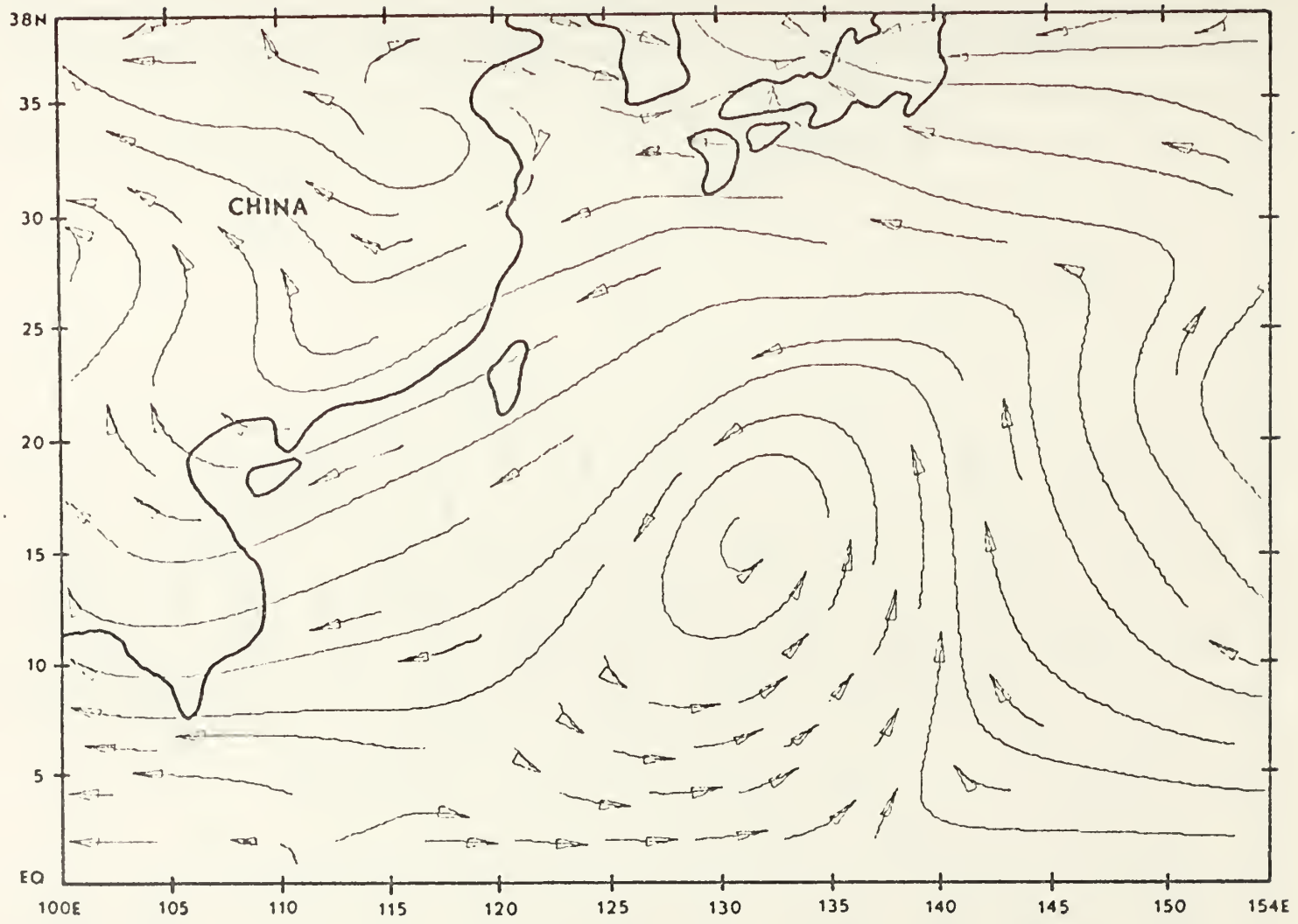

Figure 15. Nested model 24-hour 850-mb wind prognosis from 00 GMT 25 November 1974.

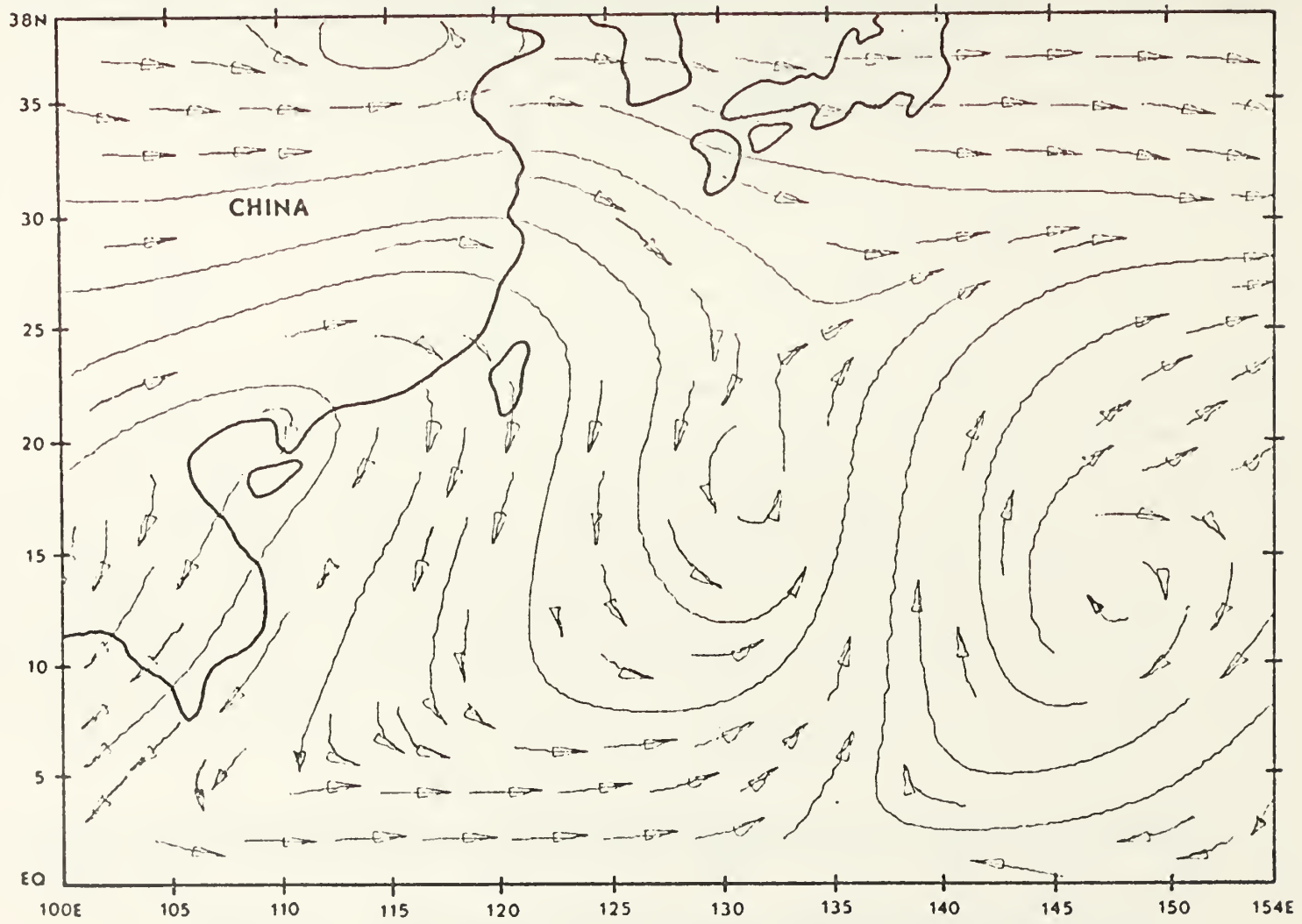

Figure 16. Nested model 24-hour 500-mb wind prognosis from 00 GMT 25 November 1974.

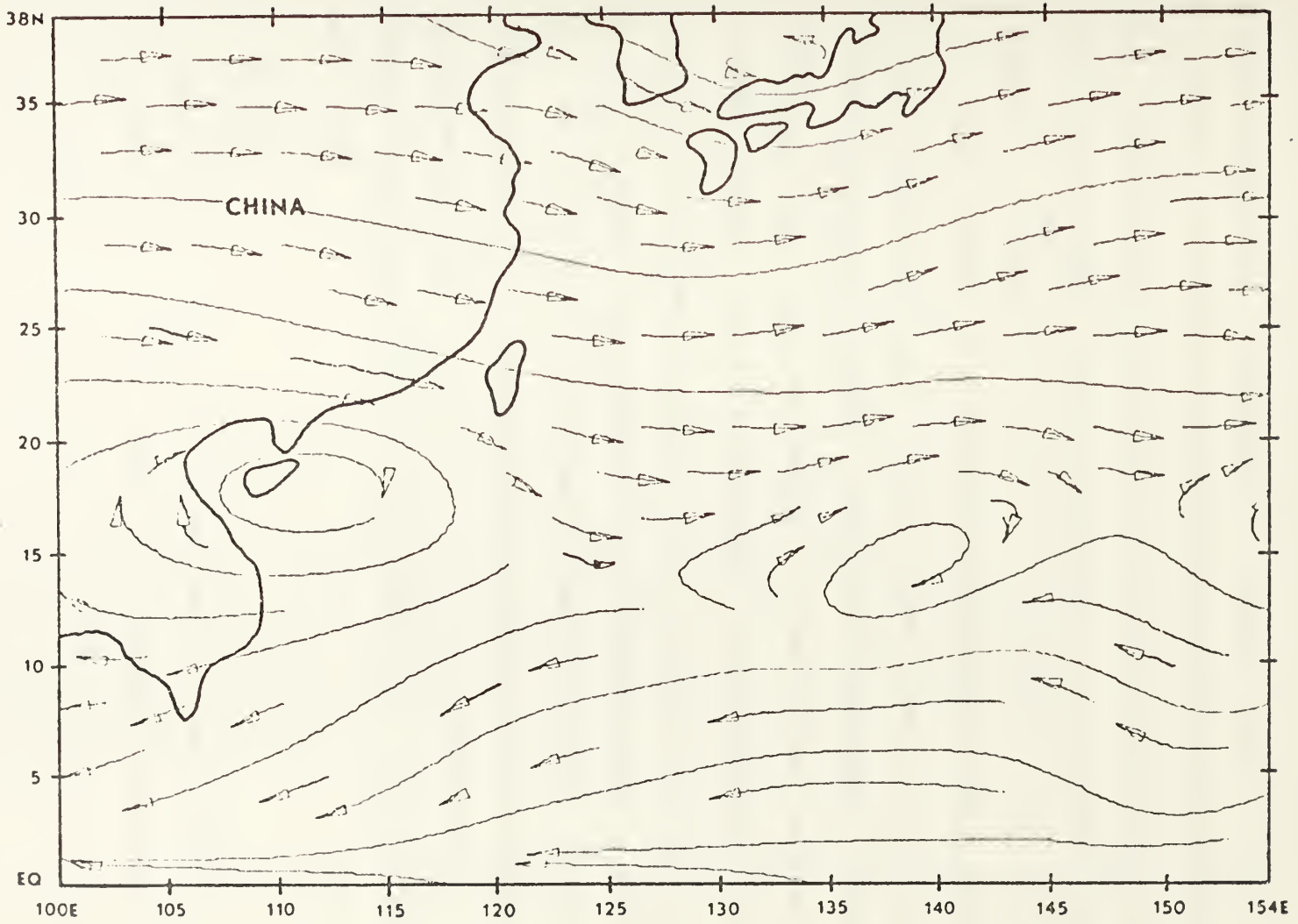

Figure 17. Nested model 24-hour 200-mb wind prognosis from 00 GMT 25 November 1974.

existed in the vertical throughout this forecast period. Vertical separation appeared to be slightly worse in the uniform CMG model, than in the nested model where the MMG and FMG tended to link the vertical structure near the storm vortex. One should note that the purpose of the study was to examine dynamic movement forecasts primarily due to advective processes, since vertical diffusion and latent heat release parameterization were omitted from the model. Numerical simulation of rain bands, the eye wall or even the intensity of the storm were not of concern in this experiment.

Lastly, the degree of interaction between Irma and the mid-latitude features should be mentioned. Mathur's (1974) movement forecast of Hurricane Isbel essentially excluded interaction of the higher latitude forcing by imposing constant dependent variables on the northern boundary. In the Harrison model, the grid movement and two-way interaction between grids allows the storm to respond to the mid-latitude forcing. Furthermore, the particular case chosen for this study represents a late-season storm when the extratropical influences are the greatest. The fact that the model successfully simulated the interaction in this advective case is encouraging; however, inclusion of latent heat parameterization and moisture to the model will be necessary before more conclusive comments can be made.

B. TRACKS

Forecasting of tropical cyclone movement is a very difficult task, and therefore requires that complete data resources and forecast tools are at the meteorologist's disposal. The primary data sources at FWC/JTWC are computer-derived tropospheric wind data, hand-analyzed charts at three atmospheric levels, detailed reconnaissance plots on sectional

charts, satellite data and radar data. Forecasting aids include analog forecasts, statistical forecasts with regression equations, extrapolation, steering by geostrophic winds at 500 mb and 700 mb and steering by global band upper air fields. These objective techniques are further supplemented by various climatological publications. Thus, the preparation of each tropical cyclone forecast by FWC/JTWC personnel entails much careful preparation and guidance from the current objective and statistical methods. The 24-, 48- and 72-hour typhoon movement and intensity forecasts are generally prepared at normal synoptic times, 00 GMT plus every 6 hours (Annual Typhoon Report, 1974).

Dynamic movement forecasts to 48 hours with the uniform CMG model and the nested model will be compared with FWC/JTWC forecast tracks and the FWC/JTWC "best" track, as determined by a detailed post-season analysis. Fig. 18 depicts dynamic and operational track forecasts from 00 GMT 25 November. FWC/JTWC forecast a recurvature track (Fig. 18, Track A), which is not surprising considering the strong break in the subtropical ridge at this time (Fig. 9). Tracks B and D, Fig. 18, are those forecast by the uniform CMG model and the nested model, respectively. While the FWC/JTWC 24-hour forecast position is about 100 nmi north of the "best" track position (Track C, Fig. 18), the uniform CMG and the nested forecast errors are considerably less, with the nested model prognostic position within 30 nmi of the verifying location. One can readily see that the 48-hour position forecast discrepancy created by the recurvature track of FWC/JTWC, might have been reduced considerably had numerical dynamic guidance been available. The uniform CMG model and nested model 48-hour forecast errors vary from about 40 nmi to near 60 nmi, with the better prognosis obtained with the uniform CMG model.

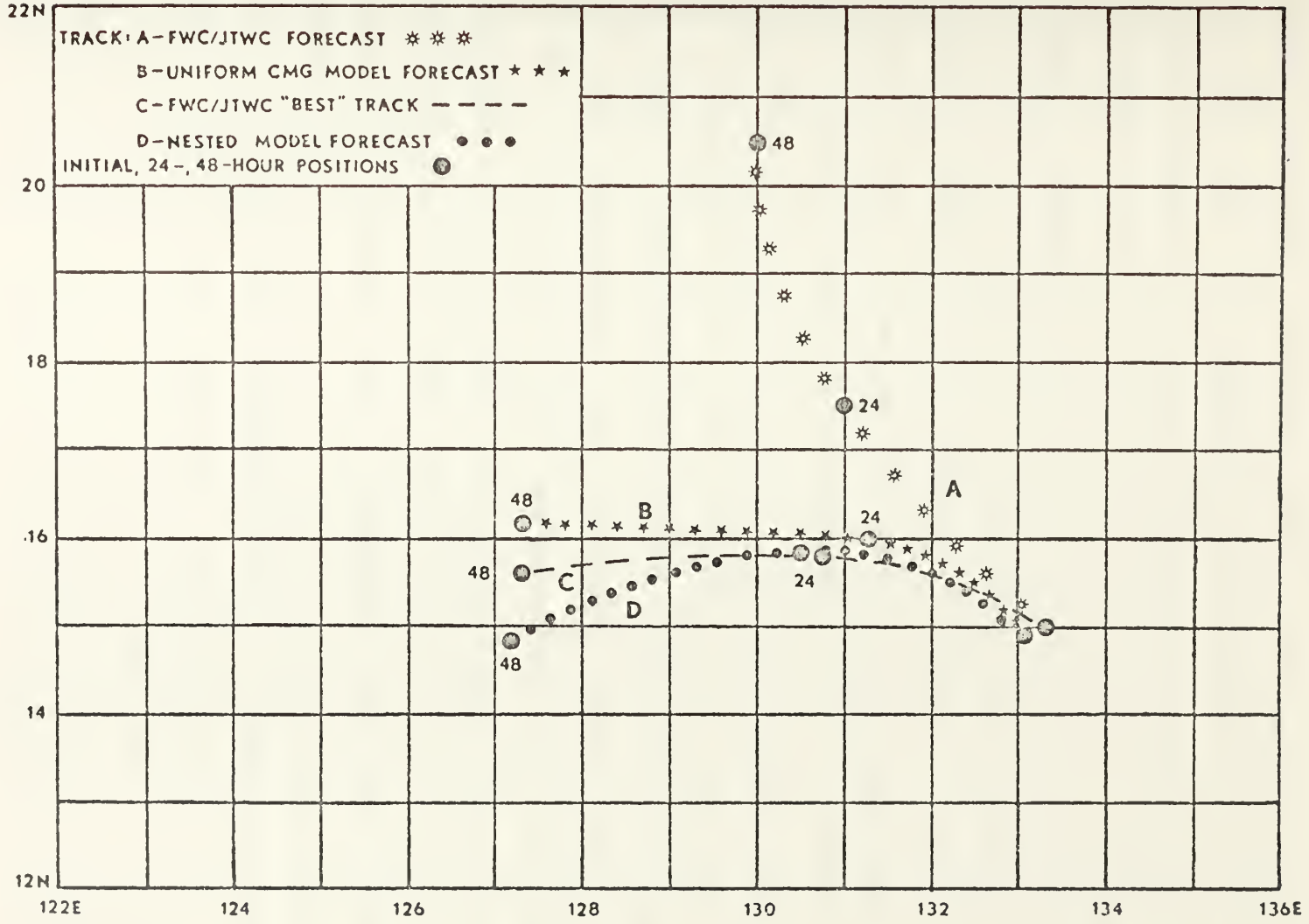

Figure 18. "Best" track, uniform CMG model, nested model and FWC/JTWC operational forecast tracks from 00 GMT 25 November 1974.

A comparison of the dynamic model prognoses, the FWC/JTWC "best" track and the FWC/JTWC forecast track from 00 GMT 26 November 1974 is presented in Fig. 19. Here deviation of about 40 nmi from the "best" track is observed in the initial position of the uniform CMG model and the nested model. This illustrates the difficulty of forcing the exact initial position onto the finite difference lattice when the FMG fields are simply linearly interpolated from the CMG analysis. The 24-hour forecast by FWC/JTWC is still a pre-recurvature track, although the slower movement indicates that a more westerly track was expected by FWC/JTWC forecasters, but was evidently not forecast to preserve continuity with the previous prognosis (based on author's previous experience). The nested model 500-mb streamfunction field at 00 GMT 26 November 1974, shown in Fig. 20, reflects a 5-7 degree northward progression of the subtropical ridge in the 24 hours between the 25th and the 26th of November. During the same time period, Irma's 500-mb vortex moved slowly west-northwestward. Thus, the easterly steering component felt by Irma on the equatorial side of the subtropical ridge should have increased. In fact, the "best" track, Track C shown in Fig. 19, reveals that Irma moved slightly south of west during the next 48 hours and accelerated from an average 6-kt movement on the 25th to 10 kts on the 26th. The uniform CMG model forecast track very nearly parallels the "best" track; but is considerably slower. A slightly faster movement is forecast by the nested model, and consequently its 24-hour forecast position is somewhat closer to the "best" track position than either the uniform CMG model forecast position or the official FWC/JTWC forecast position. Errors for the uniform CMG 24-hour forecast and the

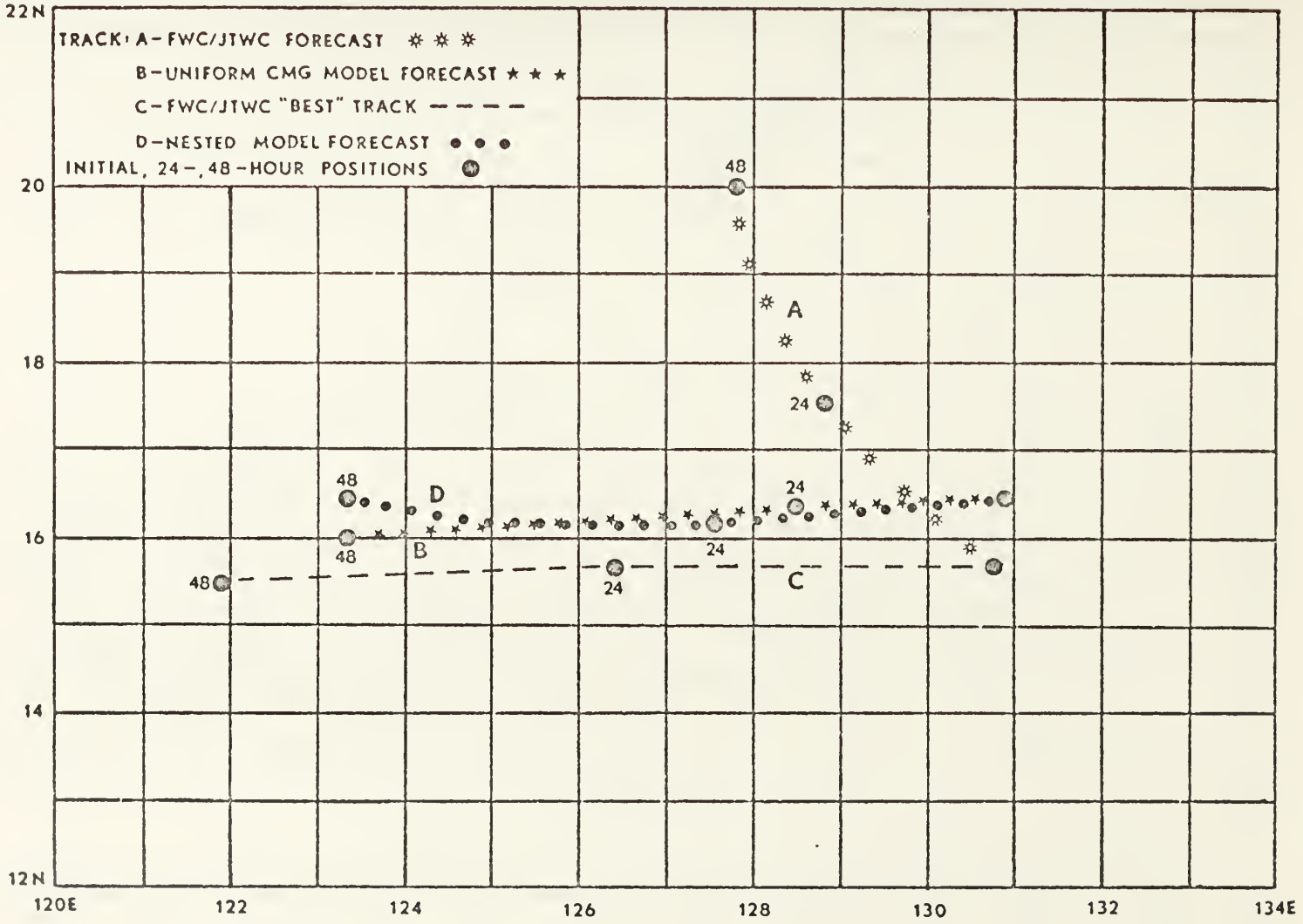

Figure 19. "Best" track, uniform CMG model, nested model and FWC/JTWC operational forecast tracks from 00 GMT 26 November 1974.

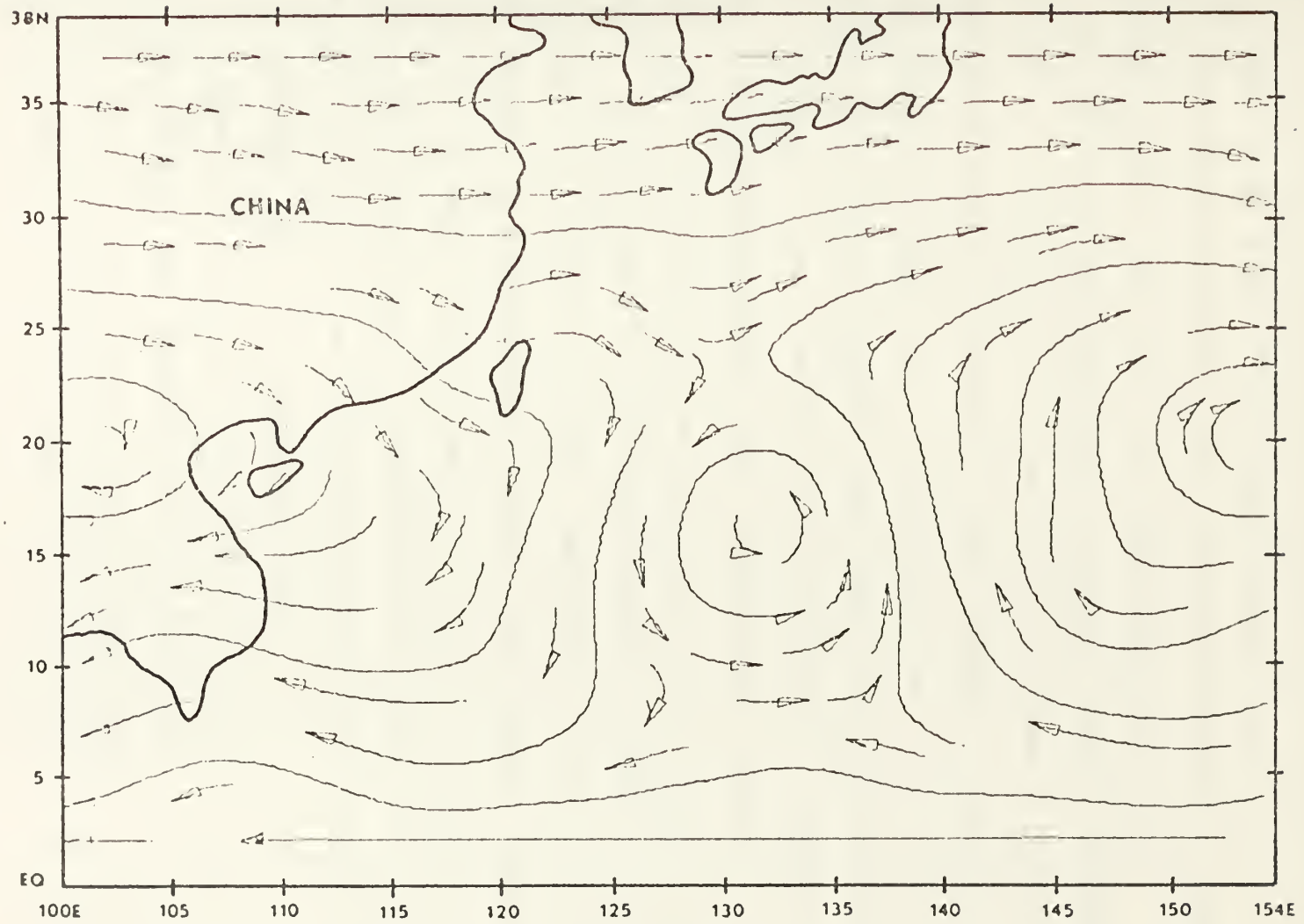

Figure 20. Nested model 500-mb streamfunction at 00 GMT 26 November 1974 (reverse telescoping).

nested model 24-hour prognoses were about 140 nmi and 90 nmi, respectively. The advantage of the nested model over the uniform CMG model is lost by 48 hours, as the nested model produced a west-northwest track as opposed to the uniform CMG model west-southwest track that paralleled closely the "best" track. The uniform CMG 48-hour error was about 90 nmi while that of the nested model approached 135 nmi.

The initial 500-mb streamfunction at 00 GMT 27 November is presented in Fig. 21. It shows continued slow northward progression of the subtropical high cells east and west of Irma. In general, however, the steering pattern appears to be very similar to that of the previous day. Dynamic guidance and the FWC/JTWC "best" track, as illustrated in Fig. 22, both exhibit a west-southwesterly storm trajectory. FWC/JTWC forecast a west-northwesterly track that resulted in 24- and 48-hour position errors of 66 nmi and 129 nmi, respectively (Annual Typhoon Report, 1974). Position errors for the uniform CMG model were about 60 nmi at 24 hours and 160 nmi at 48 hours. The uniform CMG model 24-hour forecast position is slightly better than the 24-hour prognostic position of the nested model. It is interesting that most of the dynamic models' forecast errors arose due to an erroneous speed forecast, while the FWC/JTWC speed forecast was appreciably better and the direction forecast introduced most of the positioning error.

In summary, the average 24- and 48-hour position errors for the uniform CMG model were approximately 85 nmi and 100 nmi. The same figures for the nested model were about 65 nmi and 160 nmi. FWC/JTWC 24- and 48-hour average values during this period were 115 nmi and

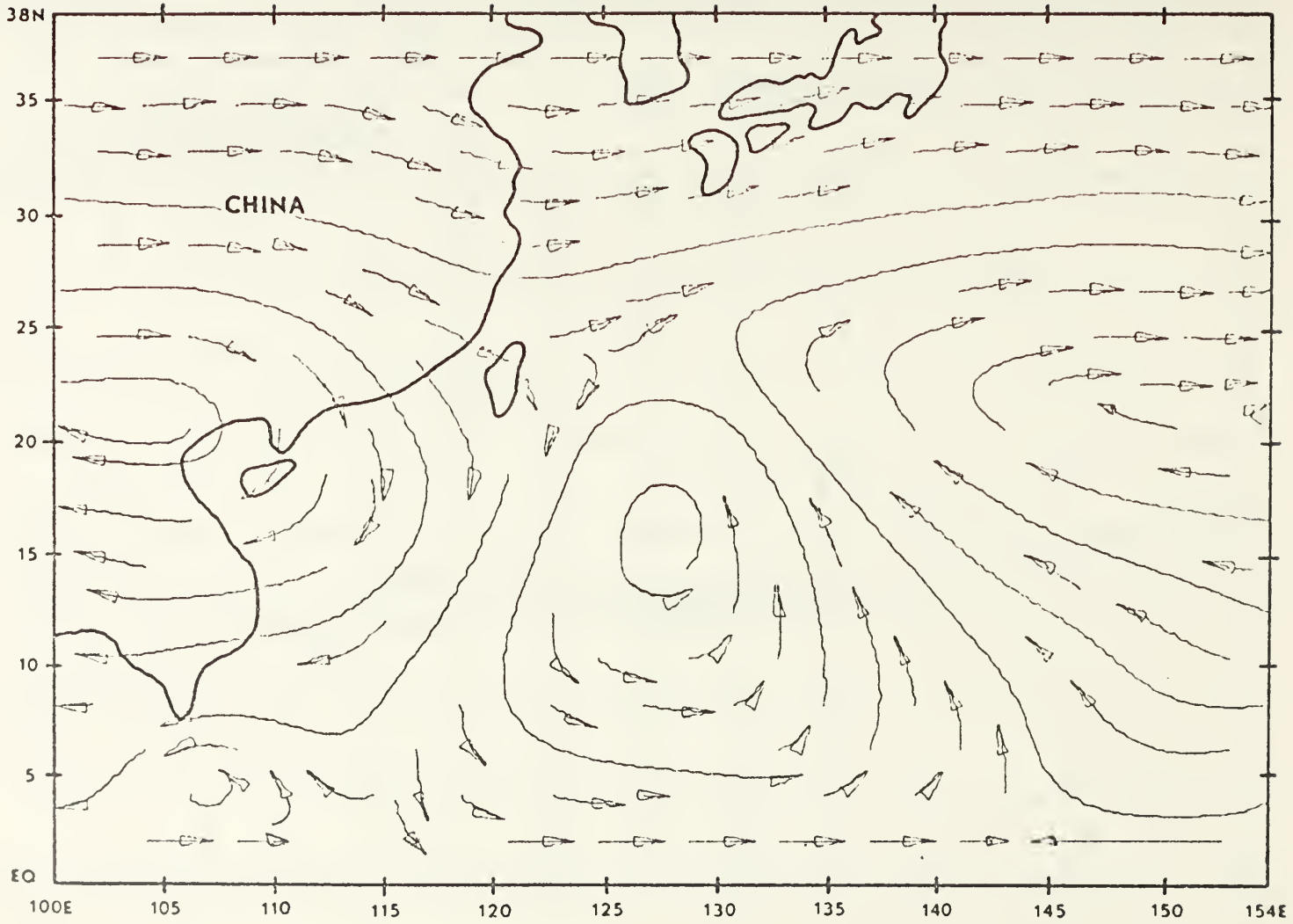

Figure 21. Nested model 500-mb streamfunction at 00 GMT 27 November 1974 (reverse telescoping).

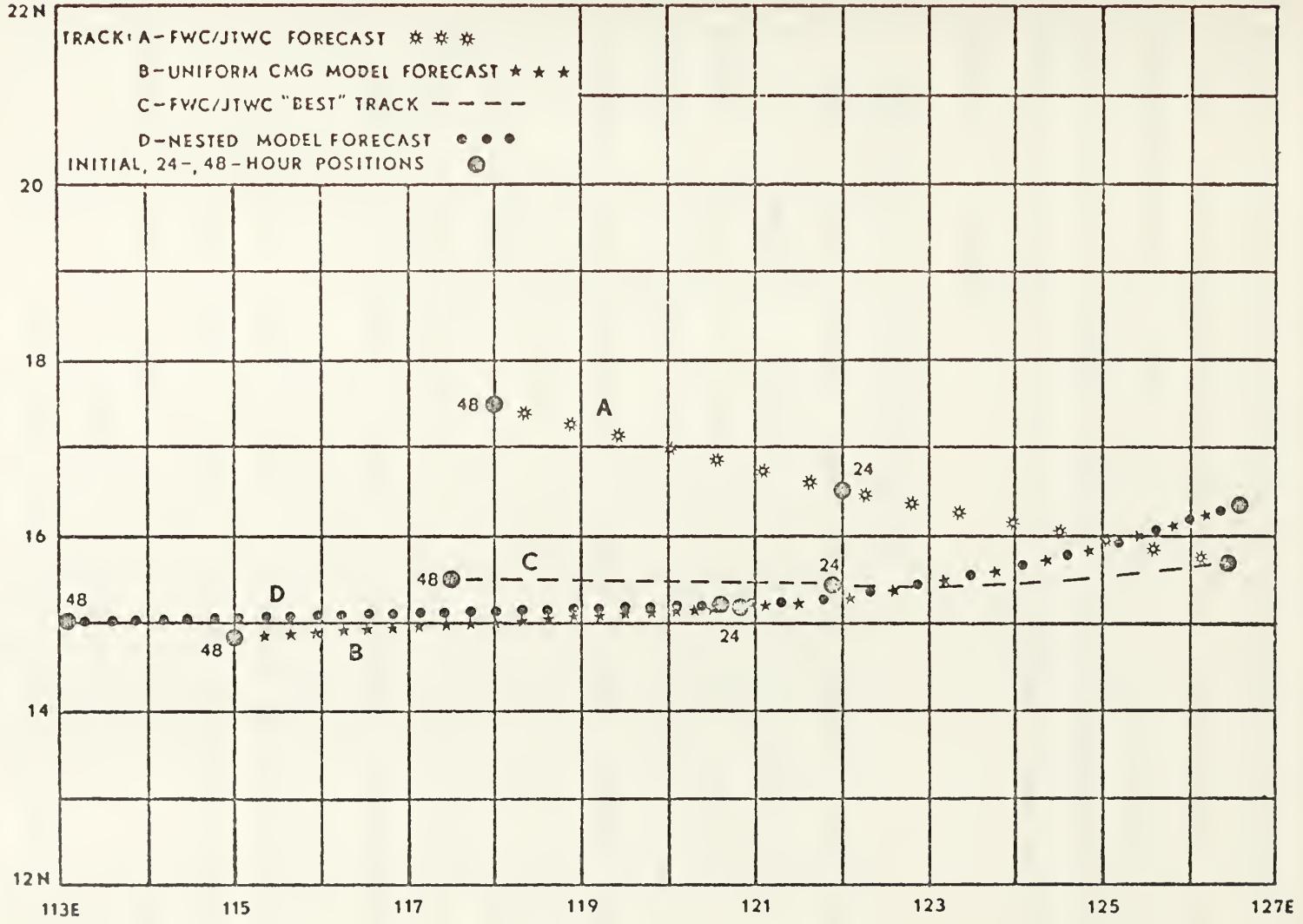

Figure 22. "Best" track, uniform CMG model, nested model and FWC/JTWC operational forecast tracks from 00 GMT 27 November 1974.

305 nmi; and for the 1974 season, 114 nmi and 218 nmi. Thus, it appears that the dynamic numerical model position forecasts during this period would have assisted operational forecasters. One should note, however, that the particular case studied here was selected to determine if the dynamic model would predict recurvature for this situation. It cannot be expected that the dynamic model would show such an improvement in every situation. Continued testing of the nested model under varied movement situations, such as recurvature, is required before definite conclusions can be reached.

C. TELESCOPING VS REVERSE TELESCOPING

Recall from the earlier chapter on initialization that linear interpolation of dependent variables from the CMG to the finer mesh grids was adequate to specify the initial data fields prior to solution of the streamfunction and balance equations. Reverse telescoping was introduced to guarantee the ultimate balance between the mass and wind fields by solution on an enlarged grid. Relaxation in the reverse direction, that is, from the FMG, to the CMG, was then necessary to assure consistency in the grid interface values used in the model's two-way interaction.

There are two benefits inherent in the reverse telescoping procedure. First, the interface boundary values are now determined by the finer mesh grid wind and height fields. As a result, the interface wind speeds in the finer mesh grids are characteristic of the higher resolution field and are not constrained by the coarser grid solution. During early steps of the integration, the interface boundary conditions are determined by the time tendency of the coarser mesh grid fields, but these tendencies are added to a finer mesh grid boundary value that is consistent with the interior field. Thus, the reverse telescoping will promote the two-way grid interaction. Second, relaxation on the enlarged grid reduces

the effect of the boundary values imposed by the CMG solution on the FMG. This allows for the best FMG dynamic balance between the mass and winds that is possible without using a fine mesh initialization everywhere. Thus, the adjustment between the mass and wind distributions, during the first few iterations,due to dynamic imbalance in the initial fields, will be minimized. By avoiding the introduction of computational modes early in the integration, contamination of the large-scale features is reduced.

The reverse telescoping procedure contributes increased resolution to the MMG through the feedback of the FMG solution. This can be seen by comparing Figs. 23 and 24, the reverse telescoped and telescoped MMG initial 1000 mb height fields at 00 GMT 27 November. Note the expansion of the 0-m and -30-m contours in the reverse telescoped field. The straight line segments of the -30-m isoline in Fig. 24 are due to the computer plotting package. Greater differences in the fields are not observed because non-linearity imposed during solution of the coarser mesh grid provides a fairly good boundary estimate to the finer mesh grid. More profound differences between the reverse telescoped and telescoped initial states may be realized in the initialization of asymmetric tropical cyclones, where non-linear gradients are observed and can only be represented by the data extraction to the coarser resolution grids.

The improvement in the nested model prognostic fields when the initial state included reverse telescoping is not easily detectable in the large-scale fields. Relatively small changes were apparent in the forecast fields, but these were masked by filtering that proceeded the computer plotting. Furthermore, most computational modes introduced

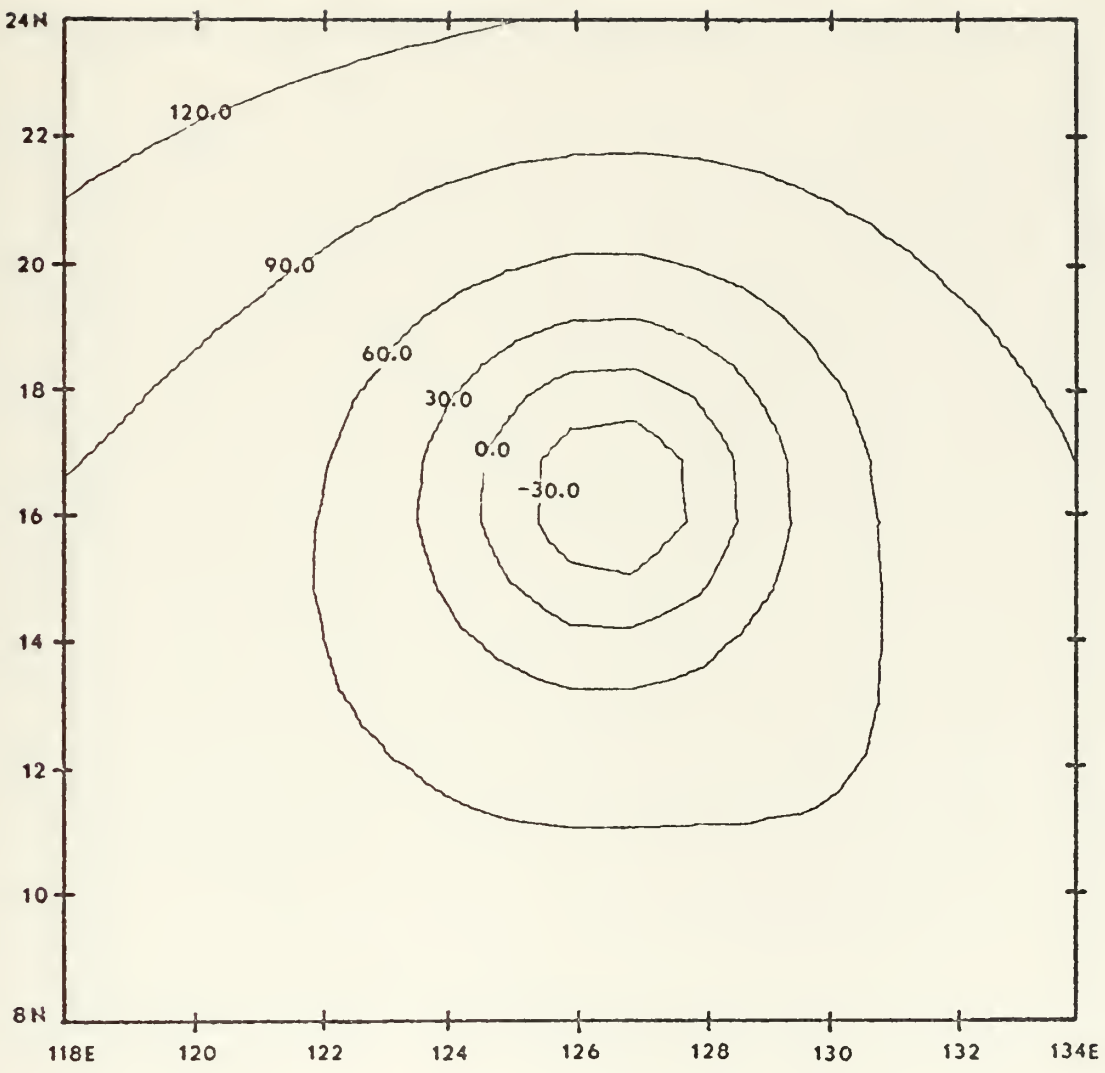

Figure 23. Nested model MMG initial 1000-mb height field at 00 GMT 27 November 1974 (reverse telescoping).

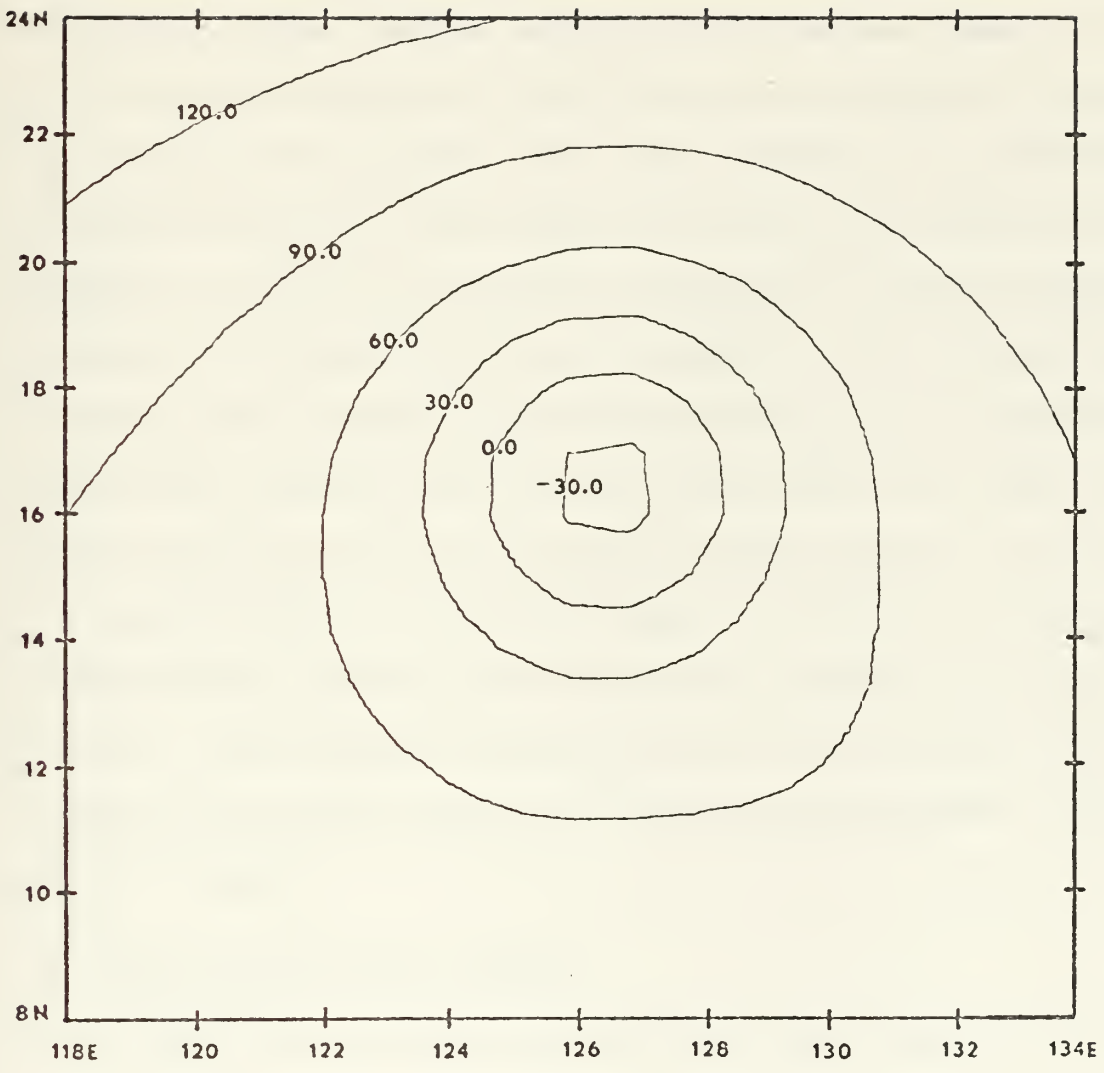

Figure 24. Nested model MMG initial 1000-mb height field at 00 GMT 27 November 1974 (telescoping).

during the initialization can be seen only in the early stages of the integration and will be dampened by 24 hours. Lastly, the model's horizontal diffusion inhibits short-wave growth and may quickly stabilize gravity modes generated during the first few time steps.

Two consequences of the reverse telescoping were readily observed in the initial data fields. First, the extraction of the winds from the finer mesh grid to the coarser grid resulted in an initial divergent component adjacent to the interface and within the coarser mesh grid area specified by the finer mesh grid solution. The resultant vertical velocities were, however, quickly dispersed early in the integration. Second, the feedback of data from the finer grids to the coarser mesh grids allows for increased compatibility between dependent variables on the three grids. Since the FMG values are extracted to the MMG, and the MMG values to the CMG, higher resolution is passed from the FMG to the CMG. This increased consistency among the grids should result in a smoother start and a reduction of gravity modes during the initial iterative steps.

D. NESTED MODEL-RELATED FEATURES

A serious model-related problem was the lattice separation in fields, since the dependent variables are carried at all grid points. This lattice separation increased throughout the integration and the "checkerboard" character of the solutions would have led to computational instability. To combat this separation, horizontal diffusion was used in the momentum equations (Eqs. (1) and (2)). The diffusion coefficients were larger than those necessary when analytical fields were used in the nested model (Harrison, 1973). The presence of horizontal diffusion

resulted in a gradual expansion of the maximum wind radius as time progressed. This occurred on all grids, and represents a type of scale interaction. By 48 hours, the FMG cyclonic flow was greatly weakened, with nearly linear wind shear present in the horizontal. Once considerable weakening in the zonal and meridional wind components was experienced, the FMG geopotential solution deteriorated. This explains why care must be taken when choosing the diffusion coefficients to be applied on the MMG and FMG. Inclusion of heating would have compensated the spurious dampening. However, it was not the intent of this research to test the various methods of latent heat parameterization which have been used in previous simulations of tropical cyclone development (see Elsberry, 1975).

Another interesting computational aspect concerned the effects of grid movement. It was mentioned previously that when the tropical cyclone minimum 1000-mb height reached a position seven grid points from the FMG western or northern boundary, the FMG was moved one MMG point in the appropriate direction. Likewise, similar provision was available to move the MMG one CMG point north or west when the FMG moved near the northern or western walls of the MMG. Each grid movement entails interpolation of new geopotential values, potential temperatures and winds from the coarser mesh grid to the leading edge of the finer mesh grid. This linear interpolation of the wind components generates imbalances between the mass and wind fields near the leading edge of the grid boundary. As the wind and mass fields adjust, gravity modes will be propagated toward the center of the grid. Therefore, it seemed advisable to minimize the number of grid movements by placing the grids so that the storm center was initially located toward the southeastern portion of the FMG, and the FMG was located near the center of the MMG.

VI. CONCLUSIONS

The three-dimensional triply nested model of Harrison (1973) was initialized using real hand-analyzed synoptic-scale data. Mass fields were forced by the winds by using a balance equation suitable for the tropics. Data on the finer mesh grids of the nested model were obtained through linear interpolation of the CMG field. The initialization of the nested model incorporated "reverse" telescoping, a procedure that provides for the optimum balance between the finer mesh wind and mass fields through use of a grid expansion during the diagnostic phase. Initialization in the reverse direction, from the FMG to CMG, was required to specify consistent dependent variables on the grid interface. This last phase is necessary to assure a smooth start of the two-way grid interaction in the model.

Latent heat and moisture parameterizations were neglected to allow for movement forecasts based primarily on advection. The intent of the study was to determine if dynamic guidance would have been of assistance in forecasting tropical cyclone movement, not to simulate the energy-related features of the tropical cyclone. Vertical diffusion was omitted from the model, but horizontal diffusion was required to control lattice solution separation that resulted because the dependent variables were carried at each grid point.

Successful movement forecasts with the nested model and a uniform coarse grid model were obtained at 24 and 48 hours from 00 GMT 25, 26 and 27 November 1974. During this period, Typhoon Irma was forecast

by FWC/JTWC personnel to recurve into the mid-latitude westerlies. However, both numerical models produced a westerly track, similar to the one actually followed by Irma. In all three cases the dynamic model could have been helpful to FWC/JTWC forecasters. The average dynamic model 24- and 48-hour position forecast errors for the three days were substantially lower than those of the operational forecasts.

Thus, if one is interested only in storm movement, it appears that the nested model may be initialized with linearly interpolated data imposed on the MMG and FMG, provided the mass and wind fields are properly balanced. Rather good storm movement was also simulated with the uniform CMG model for this case. This is especially important since the uniform CMG model incorporated the Shuman (1971) and Brown and Campana (1971) time averaging of the pressure-gradient terms. It allowed for a time step about 70% greater than the normal time step for a centered-in space and time finite difference scheme.

Close proximity of the uniform CMG model forecast positions with those of the triply nested model reflects the diffusive spindown of the MMG and FMG winds and the dependence of cyclone movement on the large-scale advective flow.

It is anticipated that future work on the model will entail incorporation of a staggered horizontal grid to eliminate lattice separation, and thus reduce the need for horizontal diffusion. Heating parameterization should be tested with the real data. But, most importantly, more case studies involving various intensity tropical cyclones under a number of types of steering flow should be completed.

APPENDIX: An Experiment Designed to Increase the Time Step of the Harrison Model

A. INTRODUCTION

The importance of a fast, efficient numerical model is manifest in the continuous research in this area. Faster machines, improved coding and computational techniques will eventually allow more sophisticated finite difference schemes to be utilized. An interesting computational scheme was introduced by Shuman (1971) and Brown and Campana (1971) and has been recently programmed for the National Meteorological Center (NMC) model.

Shuman (1971) and Brown and Campana (1971) found that replacement of the pressure gradient term of the momentum equations with a weighted time averaged version permits doubling of the maximum time step. The averaging can be described by:

$$\frac{\partial \tilde{\phi}}{\partial x} = a\left[\left(\frac{\partial \phi}{\partial x}\right)^{\tau+1} + \left(\frac{\partial \phi}{\partial x}\right)^{\tau-1}\right] + (1-2a)\left(\frac{\partial \phi}{\partial x}\right)^{\tau} \qquad \text{(A-1)}$$

where τ is an arbitrary time level and "a" is a variable coefficient between 0 and 0.25. A similar form is used in the "v" momentum equation. When a = 0.25, theoretical results indicate a doubling of the time step can be achieved. Successively smaller time step increases can be realized as the coefficient a is reduced. When a = 0, there exists no time averaging; that is, one reverts to use of the normal pressure gradient term. Experiments by Brown and Campana (1971) indicate that computational instability may arise if a = 0.25 is used. This instability can be avoided by specifying a value of "a" slightly less than 0.25 or through application of a suitable dampening mechanism.

B. PROCEDURE

Since $(\frac{\partial \phi}{\partial x})^{\tau+1}$ must be defined before Eq. (A-1) can be used, the solution order of the closed system was re-arranged to the following:

1) 1st Law of Thermodynamics

2) 1000 mb boundary condition

3) Hydrostatic equation

4) Momentum equations

5) Continuity equation

For the condition, a = 0, the rearrangement should yield the same answer as calculations using the normal equation sequence. This served as a check for programming errors.

The time averaging was programmed successively into a two-dimensional (north/south cross-section) uniform grid model, a three-dimensional uniform CMG model, a two-dimensional nested model with a five-to-one grid reduction and the three-dimensional triply nested model. Analytic initial states were imposed on all models and heating was applied on the finest grid scale of the two- and three-dimensional nested models as in Harrison and Elsberry (1972), and Harrison (1973). Model dependent averages of the ω, in the $\omega \frac{\partial \phi}{\partial p}$ term of Eq. (4), were included. Diffusion, with various coefficients, was applied in the two-and three-dimensional nested models to control lattice solution separation.

C. RESULTS

Application of the time-averaging scheme to the two-and three-dimensional non-nested models was quite successful. In the three-dimensional uniform CMG model with grid spacing of 320 km, the maximum time increment allowed by Eq. (7) is approximately 750 sec. This

assumes that the fastest gravity modes move at 300 m/sec. The time averaged model solution closely approximated the Harrison model when the time increments for the two models were 1440 sec and 720 sec, respectively. All of the uniform CMG results in the results section of the main text were obtained from the time averaged model with a time step of 800 sec. This represents a 70% increase over the maximum time increment dictated by Eq. (7), and agrees well with Schoenstadt and Williams (1975), who found that the time advantage of the time averaging scheme is reduced to 70%-80% once a mean flow is added.

Somewhat less satisfactory results were achieved when the time averaging scheme was inserted into the two- and three-dimensional nested models. Computational instability quickly destroyed solutions in both models when a time step greater than the maximum allowed by Eq. (7) was used.

The two-dimensional nested model is characterized by only one grid reduction, a factor of five from the CMG to the FMG. When time averaging led to instability, the programming was checked by excluding the FMG solution portion from the iterative procedure. The instability appeared to be caused by lattice solution separation which was reduced by inclusion of horizontal diffusion when solving the momentum equations on the FMG. However, such strong diffusion was required that the diffusive time limit offset all advantage gained through the time averaging. To avoid application of horizontal diffusion to damp the high frequency waves generated in the time averaged model, an alternative dampening mechanism was sought.

At first, it was hoped that some type of energy absorbing scheme applied near the boundary in the FMG would absorb and prevent reflection

and growth of the gravity modes. A simple filtering scheme to reduce two grid length noise of the near boundary FMG v component was applied. This filter which used the three-point formula

$$V_i = (v_{i+1} + 2v_i + v_{i-1})/4 \qquad \text{(A-2)}$$

provided no improvement. The second scheme, spongy boundaries, which allowed the FMG points adjacent to the interface to feel a percentage of the linear forcing of the CMG at the FMG boundary, also contributed little improvement.

Since an analtyic initial state was used in the three-dimensional nested grid experiments, the forcing of the solution was provided by heating on the FMG. The long term solution of Harrison's model was nearly identical to that of the time averaged model when the same time step was used in both. This seems to suggest that the FMG heating function forced the solution to an extent that the time averaging effect was eliminated. Furthermore, no time step increase beyond that dictated by Eq. (7) was achieved with the time averaging scheme in the triply nested model. Since the initiator of the computational instability appears to be the lattice solution separation, the scheme will again be tested in a staggered grid nested model. Additional work appears to be necessary before use of the time-averaging scheme is employed in a nested grid model.

REFERENCES

1. Annual Typhoon Report, 1974: Fleet Weather Central/Joint Typhoon Warning Center, Guam.

2. Anthes, R. A., 1974: Data assimilation and initialization of hurricane prediction models. J. Atmos. Sci., 31, 702-719.

3. Brown, J. and K. Campana, 1971: A New Explicit Differencing Scheme or Primitive Equations, unpublished National Meteorological Manuscript.

4. Elsberry, R. L., 1975: Feasibility of an operational tropical cyclone prediction model for the western North Pacific area. Tech. Report NPS-51Es75051, Naval Postgraduate School, 56 pp.

5. Elsberry, R. J. and E. J. Harrison, Jr., 1971: Height and kinetic energy oscillations in a limited region prediction model, Mon. Wea. Rev., 99, 883-888.

6. Haltiner, G. J., 1971: Numerical Weather Prediction. Wiley, New York, 317 pp.

7. Harrison, E. J., Jr., 1973: Three-dimensional numerical simulations of tropical systems utilizing nested finite grids. J. Atmos. Sci., 30, 1528-1543.

8. Harrison, E. J., Jr., and R. L. Elsberry, 1972: A method for incorporating nested finite grids in the solution of systems of geophysical equations. J. Atmos. Sci., 29, 1235-1245.

9. Krishnamurti, T. N., 1969: An experiment in numerical prediction in equatorial latitudes. Quart. J. Roy. Meteor. Soc., 95, 594-620.

10. Krishnamurti, T. N., 1973: Florida State University's tropical prediction model. Tellus, 25, 523-535.

11. Mathur, M. B., 1974: A multiple-grid primitive equation model to simulate the development of an asymmetric hurricane (Isbell, 1964). J. Atmos. Sci., 31, 371-393.

12. Phillips, N. A., and J. Shukla, 1974: On the strategy of combining coarse and fine grid meshes in numerical weather prediction. J. Applied Meteo., 12, 763-770.

13. Schoenstadt, A. L., and R. T. Williams, 1975: The computational stability properties of the Shuman pressure gradient averaging technique. Unpublished Naval Postgraduate School manuscript.

14. Shapiro, R., 1971: The use of linear filtering as a parameterization of atmospheric diffusion, J. Atmos. Sci., 28, 523-531.

15. Shuman, F. G., 1971: Resuscitation of an integration procedure. National Meteorological Center Office Note 54, 15 pp.

INITIAL DISTRIBUTION LIST

		No. Copies
1.	Defense Documentation Center Cameron Station Alexandria, Virginia 22314	2
2.	Library, Code 0212 Naval Postgraduate School Monterey, California 93940	2
3.	Dr. G. J. Haltiner, Code 51Ha Department of Meteorology Naval Postgraduate School Monterey, California 93940	1
4.	Dr. R. L. Elsberry, Code 51Es Department of Meteorology Naval Postgraduate School Monterey, California 93940	9
5.	Lieutenant Gary W. Ley 2304 LaSalle Drive Reading, Pennsylvania 19609	5
6.	Commanding Officer Fleet Numerical Weather Central Naval Postgraduate School Monterey, California 93940	1
7.	Department of Meteorology Naval Postgraduate School Monterey, California 93940	1
8.	Commanding Officer Environmental Prediction Research Facility Naval Postgraduate School Monterey, California 93940	2
9.	Dr. R. T. Williams, Code 51Wu Department of Meteorology Naval Postgraduate School Monterey, California 93940	1

10. Dr. S. Piacsek — 1
Code 7750
Naval Research Laboratory
Washington, D. C. 20375

11. Commanding Officer — 1
Naval Weather Service Command Headquarters
3101 Building 200
Washington Navy Yard
Washington, D. C. 20374

12. Commanding Officer — 2
Fleet Weather Central/Joint Typhoon Warning Center
COMNAVMARIANAS Box 12
FPO San Francisco 96630

13. Lieutenant Commander Edward J. Harrison, Jr. — 1
Fleet Weather Central/Joint Typhoon Warning Center
COMNAVMARIANAS Box 12
FPO San Francisco 96630

14. Lieutenant Donald E. Hinsman — 1
Fleet Numerical Weather Central
Monterey, California 93940

Thesis 182227
L618 Ley
c.1 Some design experiments for a nested grid forecast model of western Pacific tropical cyclones.